A changing hydrological regime: Trends in magnitude and timing of glacier ice melt and glacier runoff in a high latitude coastal watershed

Joanna Young[1], Erin Christine Pettit[2], Anthony A. Arendt[3], Eran Hood[4], Glen Liston[5], and Jordan Paul Beamer[6]

[1]International Arctic Research Center
[2]University of Alaska Fairbanks
[3]University of Washington
[4]Univeristy of Alaska Southeast
[5]Cooperative Institute for Research in the Atmosphere
[6]Oregon Water Resources Department

November 30, 2022

Abstract

With a unique biogeophysical signature relative to other freshwater sources, meltwater from glaciers plays a crucial role in the hydrological and ecological regime of high latitude coastal areas. Today, as glaciers worldwide exhibit persistent negative mass balance, glacier runoff is changing in both magnitude and timing, with potential downstream impacts on infrastructure, ecosystems, and ecosystem resources. However, runoff trends may be difficult to detect in coastal systems with large precipitation variability. Here, we use the coupled energy balance and water routing model SnowModel-HydroFlow to examine changes in timing and magnitude of runoff from the western Juneau Icefield in Southeast Alaska between 1980 to 2016. We find that under sustained glacier mass loss (-0.57 +/- 0.12 m w.e. a), several hydrological variables related to runoff show increasing trends. This includes annual and spring glacier ice melt volumes (+10% and +16% decade) which, because of high precipitation variability in the area, translate to smaller increases in glacier runoff (+3% and +7% decade) and total watershed runoff (+1.4% and +3% decade). These results suggest that the western Juneau Icefield watersheds are still in an increasing glacier runoff period prior to reaching 'peak water.' In terms of timing, we find that maximum glacier ice melt is occurring earlier (2.5 days decade), indicating a change in the source of freshwater being delivered downstream. Our findings highlight that even in climates with large precipitation variability, high latitude coastal watersheds are experiencing hydrological regime change driven by ongoing glacier mass loss.

A changing hydrological regime: Trends in magnitude and timing of glacier ice melt and glacier runoff in a high latitude coastal watershed

Joanna C. Young[1], Erin Pettit[2,3], Anthony Arendt[4], Eran Hood[5], Glen E. Liston[6], Jordan Beamer[7]

[1]Geophysical Institute, University of Alaska Fairbanks, Fairbanks, AK, USA
[2]Department of Geosciences, University of Alaska Fairbanks, Fairbanks, AK, USA
[3]College of Earth, Ocean, and Atmospheric Sciences, Oregon State University, OR, USA
[4]Applied Physics Laboratory, Polar Science Center, University of Washington, Seattle, WA, USA
[5] Environmental Science Program, University of Alaska Southeast, Juneau, AK, USA
[6]Cooperative Institute for Research in the Atmosphere, Colorado State University, Fort Collins, CO, USA
[7]Oregon Water Resources Department, Salem, OR, USA

Key Points:

- Discharge from western drainages of Juneau Icefield is increasing and has yet to pass 'peak water' as glaciers lose mass
- Annual glacier ice melt volumes have increased by 10% per decade, glacier runoff by 3%, and total runoff by 1.4%
- Peak glacier ice melt volumes are increasing and arriving earlier, with impacts for downstream ecosystem function

Corresponding author: Joanna C. Young, `jcyoung6@alaska.edu`

Abstract

With a unique biogeophysical signature relative to other freshwater sources, meltwater from glaciers plays a crucial role in the hydrological and ecological regime of high latitude coastal areas. Today, as glaciers worldwide exhibit persistent negative mass balance, glacier runoff is changing in both magnitude and timing, with potential downstream impacts on infrastructure, ecosystems, and ecosystem resources. However, runoff trends may be difficult to detect in coastal systems with large precipitation variability. Here, we use the coupled energy balance and water routing model SnowModel-HydroFlow to examine changes in timing and magnitude of runoff from the western Juneau Icefield in Southeast Alaska between 1980 to 2016. We find that under sustained glacier mass loss (-0.57 ± 0.12 m w.e. a^{-1}), several hydrological variables related to runoff show increasing trends. This includes annual and spring glacier ice melt volumes (+10% and +16% decade^{-1}) which, because of high precipitation variability in the area, translate to smaller increases in glacier runoff (+3% and +7% decade^{-1}) and total watershed runoff (+1.4% and +3% decade^{-1}). These results suggest that the western Juneau Icefield watersheds are still in an increasing glacier runoff period prior to reaching 'peak water.' In terms of timing, we find that maximum glacier ice melt is occurring earlier (2.5 days decade^{-1}), indicating a change in the source of freshwater being delivered downstream. Our findings highlight that even in climates with large precipitation variability, high latitude coastal watersheds are experiencing hydrological regime change driven by ongoing glacier mass loss.

1 Introduction

Meltwater from glaciers plays a crucial and varied role in both the hydrological and ecological regimes of high latitude coastal regions around the world. From a hydrological perspective, glaciers act as frozen freshwater reservoirs, with the ability to temporarily store water over diurnal, seasonal, and long-term (decadal to millennial) time scales [*Jansson et al.*, 2003]. Watersheds containing even as little as 5% glacier cover exhibit modified flow patterns compared to their ice-free equivalents, with lower annual and monthly variability, and with a maximum seasonal flow contemporaneous not with spring snowmelt but with peak temperatures in mid-summer [*Fountain and Tangborn*, 1985]. These differences arise because while runoff from non-glacierized watersheds is dominated by precipitation, glacierized basins are primarily energy balance dominated [*Lang*, 1986].

Additionally, watersheds downstream of glaciers with persistent negative net mass balance display a distinct long-term streamflow pattern. This pattern is characterized initially by increasing discharge due to higher rates of glacier mass loss up until a maximum (often referred to as 'peak water' [*Gleick and Palaniappan*, 2010]), followed by decreasing discharge due to shrinking glacier area and volume [*Jansson et al.*, 2003]. Whether or not a particular glacierized basin or region has passed peak water is linked to several factors. *Huss and Hock* [2018] found through a global glacier mass balance modeling study that characteristics such as percent ice cover and absolute glacier size exhibit controls over the timing of peak water in a basin. Similarly, *Moore et al.* [2009] identified geographic variations in runoff trends for Western North American glacierized basins, whereby basins with larger glaciers in the north still show increasing runoff while basins with smaller glaciers further south have already passed the point of peak water. On the other hand, another study by *Carnahan et al.* [2018] identified through glacier flow modeling that glacier dynamics (characterized by glacier response times, linked primarily to climate and slope) and landscape evolution (i.e. vegetation succession after deglaciation) had a roughly equal impact on basin runoff in response to glacier retreat. Together, these findings indicate that peak water is likely to occur at different times in different regions.

Knowing whether an area is pre- or post-peak water is crucial information in glacierized watershed hydrology, due to the implications of increasing or decreasing runoff for downstream concerns such as infrastructure, ecosystems, and ecosystem resources [*Moore* *et al.*, 2009]. In a study that forecast glacier streamflow to 2100, the large glaciers of the Gulf of Alaska were predicted to experience peak water the latest (between 2060 and 2070) of all regions globally [*Huss and Hock*, 2018]. However, the fate of individual glacierized watersheds within this region was less certain due to large intrabasin variability and calibration to regional glacier mass balance observations rather than local runoff measurements.

Within the Gulf of Alaska region lies the Juneau Icefield, one of the largest icefields in North America. This area experiences extreme amounts of precipitation characteristic of maritime climates [*Pelto et al.*, 2013], and among the highest variability in precipitation of any climatic zone in Alaska [*Bieniek et al.*, 2014], both of which may act to obscure runoff trend detection. The icefield is directly adjacent to the city of Juneau, Alaska, and is closely connected to both the community's infrastructure (via bridges over glacial rivers and residential areas prone to flooding from glacial outburst floods) as well as to the downstream riverine and nearshore marine environments.

From an ecological perspective, freshwater from glaciers – whether from melted glacier ice, melted firn, or terrestrial water that has passed through a glacier system – carries a unique biogeochemical signature relative to other freshwater sources. For example, glacier runoff has been found to control fluxes of limiting nutrients crucial for primary productivity in riverine and marine environments. A previous study on streams discharging the Juneau Icefield found that glaciers serve as an important source of phosphorus and nitrogen in those streams [*Hood and Scott*, 2008], while nearby rivers such as the Copper River have proven a critical source of iron to the Gulf of Alaska [*Crusius et al.*, 2011]. Glacier meltwater also serves as a major source of bioavailable organic carbon to both riverine food webs [*Fellman et al.*, 2015] and near-shore marine ecosystems [*Hood et al.*, 2009; *Lawson et al.*, 2014]. Moreover, glacier runoff possesses physical properties that are distinct from other terrestrial water sources. In comparing several Juneau Icefield watersheds, *Hood and Berner* [2009] show that both summer stream turbidity and water temperature can be predicted by the percentage of glacier cover within the basin. These physical conditions are in turn critical for biological productivity at all trophic levels, including for Pacific salmon (*Oncorhynchus* spp.) for which stream temperature and clarity are key variables for species distribution in the north Pacific [*Welch et al.*, 1998] as well as spawning ground selection [*Lorenz and Filer*, 1989].

To assess changes in this physical landscape, several studies have evaluated glacier mass balance of the Juneau Icefield in recent decades. These have primarily relied on geodetic approaches (e.g. digital elevation model differencing) that determine bulk volume loss between two known dates. Despite sourcing imagery from different satellite sensors and covering different time spans, all studies calculated negative glacier-wide mass balance rates over the investigated periods between 1962 to 2016 [*Larsen et al.*, 2007; *Berthier et al.*, 2010; *Melkonian et al.*, 2014; *Berthier et al.*, 2018]. A recent study has also modeled future glacier mass balance for the icefield under different climate scenarios, projecting a volume loss of 58 to 68% of the icefield by 2100 [*Ziemen et al.*, 2016]. This estimate falls on the upper end of regional projections of a 32 to 58% loss of Gulf of Alaska glaciers as a whole [*Hock and Huss*, 2015].

Given the aforementioned close coupling to surrounding ecosystems and infrastructure, and its persistent state of negative mass balance, the purpose of this study is to examine whether and how components of runoff from the western Juneau Icefield have changed over the past several decades. In particular, we leverage a distributed, high-resolution model to evaluate: 1) trends in the annual or seasonal volume of total runoff, glacier runoff, and glacier ice melt; 2) shifts in timing of the onset or end of glacier runoff and/or ice melt season; 3) shifts in winter glacier runoff events or volume, and 4) changes in timing or magnitude of total runoff, glacier runoff, and glacier ice melt. This study is the first to examine recent changes in timing and magnitude of different hydrological cycle variables in this region and, in turn, to assess whether trends of increasing or decreasing runoff can be detected in a high latitude maritime environment. These findings provide key information for socio-ecological systems downstream, and leave us better poised to project future changes in ongoing climate change.

2 Study area

Bordered by mountain ranges spanning from sea level to >5000 m a.s.l., and with a maritime climate that delivers an average of 2 m w.e. and a peak of 7 m w.e. of precipitation per year [*Daly et al.*, 2008], the Gulf of Alaska coastline is characterized by both extensive glacier cover and extreme volumes of freshwater runoff. Unlike other major watersheds in North America that are dominated by large rivers, 78% of runoff into the Gulf of Alaska is delivered from the steep topography to the coast via short (~10 km average), small drainages [*Neal et al.*, 2010]. In coastal Alaska, glacier termini often lie below treeline, placing glacier ice directly adjacent to the mixed forest of the northern Pacific temperature rainforest. Together, these qualities set up a tight coupling between ice and snowmelt from alpine terrain and the nearshore marine ecosystems downstream.

The Juneau Icefield (Figure 1), centered at 58.9° N and 134.2° W, spans the coast mountains between Southeast Alaska, USA, and Northwestern British Columbia, Canada. It is the third largest icefield in North America with an area of >3700 km^2 and elevations ranging from sea level to ~2300 m a.s.l [*Kienholz et al.*, 2015]. All outlet glaciers are currently lake- or land-terminating although, as it finishes a tidewater glacier cycle advance [*Truffer et al.*, 2009], the large (~725 km^2) Taku Glacier is ~60% protected by a shoal moraine with the remaining portion of the terminus abutting a proglacial lake and short river.

Although the highest elevations receive snowfall throughout the year, C-band synthetic-aperture radar reveals that snow and/or ice melt occurs over the entire icefield during July and August [*Ramage et al.*, 2000]. Moreover, because temperatures frequently hover near the freezing point on the coast, low elevations may see ice melt and rain throughout the year. In addition to typical patterns of increasing precipitation with elevation, the icefield also experiences a strong decreasing precipitation gradient from southwest to northeast (i.e. with increasing distance from the coast) due to the prevalence of southwesterly weather systems moving inland from the Gulf of Alaska [*Royer*, 1998; *Stabeno et al.*, 2004]. These patterns are evidenced both in measurements [*Pelto et al.*, 2013] and mass balance modeling studies [*Ziemen et al.*, 2016; *Roth et al.*, 2018].

The spatial domain in this study comprises all terrain draining the western portion of the Juneau Icefield directly to the coast. Though we calculate glacier mass balance for the entire icefield for purposes of calibration, we focus our calculations and analysis of runoff on those watersheds of the icefield that supply direct runoff to marine ecosystems. This amounts to a spatial domain of 6405 km^2, of which 2860 km^2 or 44% is glacier ice covered.

3 Data & Methods

In remote and rugged settings where the availability of ground observations is scarce and long-term hydro-climatic monitoring stations are few, glacio-hydrological models can help fill knowledge gaps about the hydrological regime at high spatial and temporal resolution. To estimate glacier mass balance and total runoff at a daily time step for water years 1981 to 2016 for the Juneau Icefield, we use the energy and mass balance model SnowModel [*Liston and Elder*, 2006a], coupled with the SoilBal routine for calculating evapotranspiration over all ice-free domains [*Beamer et al.*, 2016], and the linear reservoir runoff routing model HydroFlow [*Liston and Mernild*, 2012]. These model routines, including sub-modules we used, are described below, as are the data and approaches used for initialization, calibration, and validation.

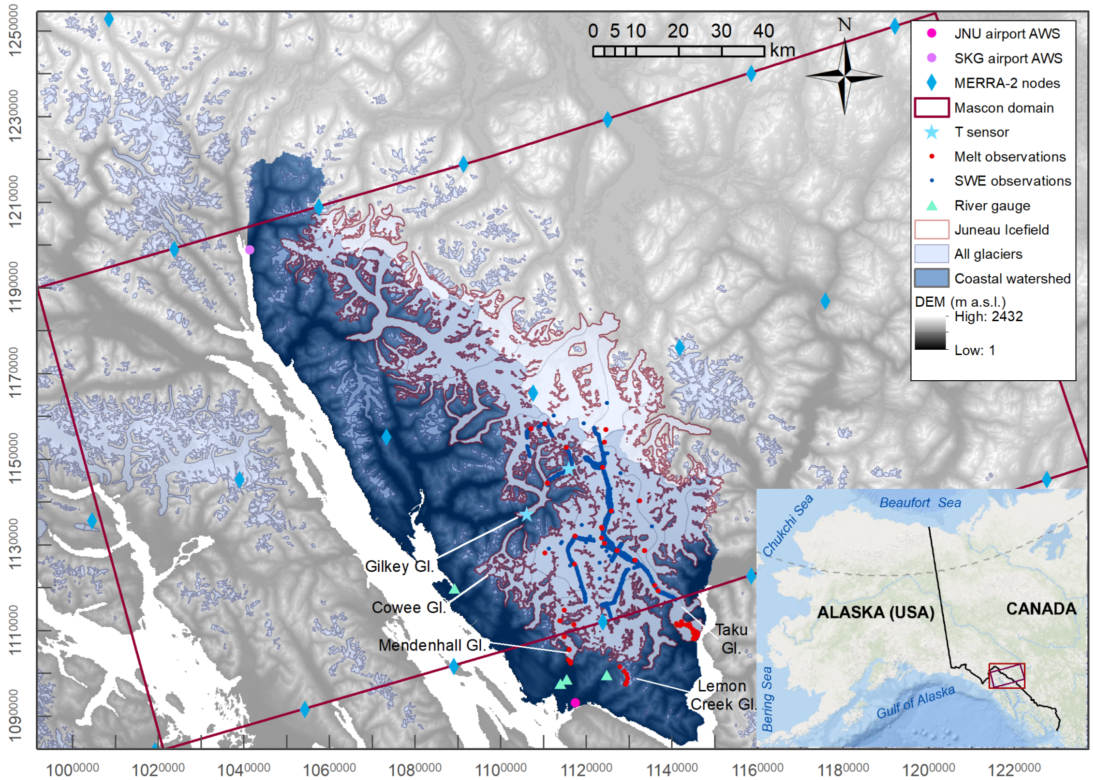

Figure 1. Location of the Juneau Icefield within the Coast Mountains spanning southeast Alaska and northern British Columbia. All glaciers within the rectangular model domain are shown in light blue, and the contiguous glaciers of the Juneau Icefield as defined in the Randolph Glacier Inventory version 6.0 are outlined in red. Also shown are: locations of automated weather stations at each the Juneau (JNU) and Skagway (SKG) airports; MERRA-2 reanalysis climate nodes; the mascon domain showing the area of GRACE solutions used for model validation; campaign on-ice temperature sensors; observations of melt and snow water equivalent (SWE); and stream gauge stations. Terrain shown in dark blue indicates the spatial extent of our coastal watershed domain for this study.

3.1 Model description

3.1.1 SnowModel

SnowModel is a distributed energy and mass balance model for simulating snow distribution and evolution in terrain where snow and ice are present [*Liston and Elder*, 2006a]. It uses meteorological, elevation, and surface type data as inputs, and accounts for all first-order processes involved in snowpack evolution, including: snow accumulation; forest canopy interception, unloading, and sublimation; snow-density evolution; and snowpack and ice melt. SnowModel is comprised of several sequential sub-routines: 1) MicroMet, 2) EnBal, and 3) SnowPack.

MicroMet is a quasi-physically-based data assimilation and interpolation routine that distributes coarse-resolution meteorological forcing over high-resolution topography [*Liston and Elder*, 2006b]. MicroMet adjusts coarse-resolution climate data in two ways: a) all available data are spatially interpolated over the domain, and b) physical submodels are applied to each variable to generate more realistic values at each grid cell and time step. MicroMet also estimates solar and incoming longwave radiation based on topography and cloud cover based on relative humidity and temperature.

EnBal performs surface energy balance calculations at every grid cell, in response to atmospheric conditions generated in MicroMet. Energy terms are added at the snow- or ice-atmosphere interfaces, and any surplus energy is assumed to be available for snowmelt, or for glacier ice melt once overlying snow has been removed [*Mernild et al.*, 2006].

SnowPack simulates snow depth and snow water equivalent evolution within the snowpack based on precipitation and melt energy. Snow density changes in response to snow temperature and the weight of overlying snow, as well as by snow melting and rain-on-snow events, which redistribute water through the snowpack. Further details on both EnBal and SnowPack are available in *Liston and Elder* [2006a], and on MicroMet in *Liston and Elder* [2006b].

SnowModel does not include a glacier flow model to redistribute mass under climate forcing. To avoid infinite snow accumulation at high elevations over glacier cells during multi-year simulations, each year's end-of-summer snowpack over glacier cells is reset to zero under the assumption that residual snow is converted to glacier ice. SnowModel also does not account for changes in either glacier extent by retreat or hypsometry (area-altitude distribution) by thinning or ice flow and instead keeps a constant surface and extent representing conditions during a reference year/period (Section 3.2.1). See Section 6 for further examination of this limitation. Moreover, while SnowModel includes many internal processes within the snowpack related to density changes and meltwater percolation, it neglects snow and ice mass loss due to dynamic processes, such as frictional melting from viscous heating (internal deformation of the ice) or sliding at the glacier bed [*Mernild et al.*, 2014].

SnowModel has been applied in a number of Arctic glaciology investigations at similar spatial scales as our study, including in Alaska and Greenland [*Liston and Sturm*, 2002; *Mernild et al.*, 2006, 2007, 2010; *Liston and Hiemstra*, 2011; *Mernild et al.*, 2015, 2017]. Recently, SnowModel has also been applied along with the SoilBal and HydroFlow routines to model freshwater discharge from 1980 to 2014 for all terrain draining into the Gulf of Alaska [*Beamer et al.*, 2016], a study which informs several of our model configuration choices.

3.1.2 SoilBal

SoilBal, a soil moisture submodel, was developed by *Beamer et al.* [2016] to formally introduce evapotranspiration (ET) into the SnowModel-HydroFlow process, in order to allow for full water balance calculations over ice-free landscapes, including vegetation. SoilBal first calculates potential evapotranspiration (PET) by means of the Priestley-Taylor equation, which is based on the concept that an air mass moving over a vegetated landscape with abundant water will become water saturated [*Priestley et al.*, 1972]. It uses only daily air temperature and net radiation for the top of the canopy as input data, making it more computationally efficient than complex formulations that include aerodynamic terms. The Priestley-Taylor formulation has been applied to many types of forested landscapes (see *Komatsu* [2005] for a review of studies) and has been found to outperform more complex formulations for a mixed temperate mountainous forest [*Shi et al.*, 2008]. After PET is calculated, a soil water balance [*Hoogeveen et al.*, 2015] is solved using inputs of PET, runoff from SnowModel, and gridded soil water storage. SoilBal ultimately produces daily grids of actual evapotranspiration, surface, and base flow runoff. The latter two are summed and used to drive the water routing model HydroFlow.

3.1.3 HydroFlow

Using instantaneous water balance information from SnowModel and SoilBal, the HydroFlow model simulates the routing of surface runoff from rainfall, snow, and ice melt to downslope areas and ultimately to basin outlets or surrounding oceans [*Liston and*

Mernild, 2012; *Mernild and Liston*, 2012]. In HydroFlow, each grid cell acts as a linear reservoir (i.e. a reservoir with discharge linearly proportional to water input) that transfers water from itself and any upslope cells to the downslope cell, creating a topographically linked flow network. HydroFlow assumes that within each grid cell there are two transfer functions with two time scales, each associated with different water routing mechanisms. Runoff enters first into the slow-response reservoir, which accounts for the time it takes for water transport through the snow, ice, and soil matrices. The moisture is then routed through the flow network via the fast-response reservoir, which generally represents some form of channel flow, such as supra-, en- or subglacial flow, or streamflow. Residence time coefficients for each reservoir in each grid cell are a function of many elements, including: surface slope; snow, ice, and soil porosity; snow temperature (cold content); density of glacier crevasses and moulins; hydrostatic water pressure; and soils and land-cover characteristics. HydroFlow therefore assigns residence time coefficients and velocities for four dominant surface types that account broadly for these processes: snow-covered ice, snow-free ice, snow-covered land, and snow-free land. A coupled system of equations solves for slow- and fast-response flow, yielding a discharge hydrograph for each grid cell. A full description of HydroFlow is available in *Liston and Mernild* [2012].

3.2 Model configuration

Our model simulations cover the water years between Oct. 1, 1980 to Sept. 30, 2016 and are run using a daily time step and grid cell size of 200 m x 200 m. The chosen temporal and spatial resolution represent a compromise between the desired level of detail and computational efficiency, given the large spatial domain.

Figure 1 shows our model spatial domain, which encompasses the full extent of all observational datasets used for calibration and validation (described below). For this study's results and interpretation, unless otherwise specified, reported findings on glacier mass balance include model grid cells within the red outline of the Juneau Icefield, in order to match estimates from both *Berthier et al.* [2018], used in model calibration, and *Ziemen et al.* [2016], which we refer to in our discussion of future changes. However, when reporting findings on freshwater runoff, we include in our spatial domain all terrain with Juneau Icefield glacier ice in its headwaters that drains directly to the coast. We do not include terrain that routes freshwater into large interior rivers (Taku River, with a drainage area of 17,000 km^2, and the Yukon River, 850,000 km^2). We exclude these regions for two reasons. First, the size of these river drainages is sufficiently different than the short, steep coastal drainages of the western portion of the Icefield (e.g. the basin drained by the Mendenhall River is the largest at 289 km^2) and therefore exemplify different watershed processes. Second, Taku and the Yukon drain primarily continental terrain subject to a different climatological regime, given that they lie in (and well beyond) the rainshadow of the Coast Mountain range that creates a strong precipitation gradient from coast to interior [*Roth et al.*, 2018]. We focus our analysis and discussion on the unique hydrological regime of the short and steep coastal drainages, particularly given their relevance to downstream estuary conditions, and their prevalence throughout high latitude coastal regions in Alaska (e.g. Glacier Bay, Prince William Sound) and beyond (e.g. Patagonia, New Zealand, Norway).

To evolve the snowpack and route water through the landscape, SnowModel-HydroFlow requires topographical data, land cover information, and meteorological forcing.

3.2.1 Elevation, land cover, and soil type

For model simulations, we use a digital elevation model (DEM) from the United States Geological Survey (USGS) National Elevation Dataset (available at https://nationalmap.gov/elevation.html), representing elevations from the early 2010s as measured by Interferometric Synthetic Aperture Radar data. Elevation data are available at a resolution of 1 arcsec (~30 m) over ~95% of the domain, and 2 arcsecs (~60 m) over portions of Canada for which data at a better resolution are not available. The DEM is hydrologically corrected (i.e. depressionless) and we resample to 200 m resolution using a nearest-neighbor sampling technique. Note that we do not modify glacier surface elevations or extents through the 1980 to 2016 model period given that earlier DEMs for the full icefield are not available.

Land cover classes are obtained from the 2011 North American Land Change Monitoring System (NALCMS), which distinguishes vegetation class, bare land, and urbanized area for North America at a 30 m resolution [*Homer et al.*, 2015]. We resample to 200 m and align the grid with our DEM and reclassify to the vegetation classes defined in *Liston and Elder* [2006a]. To delineate glacierized terrain, we modify the NALCMS grid using higher precision glacier outlines derived from the mid-2000s from the Randolph Glacier Inventory (RGI) v6.0, available at https://www.glims.org/RGI/rgi60_dl.html [*Pfeffer et al.*, 2014; *Kienholz et al.*, 2015]. Note that over our model period, we do not update surface type information related to e.g. vegetation succession after deglaciation, due to a lack of information on glacier and vegetated area extent dating back to the 1980s.

To classify soil types, we use the gridded Harmonized World Soil dataset version 1.2 (available at http://www.fao.org/soils-portal/soil-survey/soil-maps-and-databases/harmonized-world-soil-database-v12/en/) [*Fischer et al.*, 2008], which we resample from its native 1 km resolution to 200 m using a nearest-neighbor technique.

For the SoilBal soil moisture module, we use a Priestley-Taylor coefficient of 1.26, a value found by *Beamer et al.* [2016] to reproduce modeled ET for the Gulf of Alaska that most closely matches independent estimates from the Moderate Resolution Imaging Spectroradiometer (MODIS) satellite product as found in *Hill et al.* [2015].

3.2.2 Meteorological data

For meteorological forcing, SnowModel requires daily temperature, relative humidity, wind speed and direction, and precipitation. We use reanalysis data from NASA's Modern-Era Retrospective Analysis for Research and Applications, Version 2 (MERRA-2) [*Gelaro et al.*, 2017], available at http://gmao.gsfc.nasa.gov/reanalysis/MERRA-2/. One of our principal motivators in choosing this product is that in their modeling study on freshwater runoff to the Gulf of Alaska, *Beamer et al.* [2016] found that Version 1 of MERRA [*Rienecker et al.*, 2011] performed best in reproducing measurements of point glacier mass balance and local domain streamflow, compared to the Climate Forecast System Reanalysis *Saha et al.* [2010] and North American Regional Reanalysis [*Mesinger et al.*, 2006]. Version 1 of MERRA was also among the top products for consistency with observations of 2 m air temperature and precipitation [*Lindsay et al.*, 2014], and compared best to observed extreme precipitation days at the Juneau airport [*Lader et al.*, 2016], in two studies that compared different climate products for the Arctic and Alaska, respectively. Moreover, MERRA-2 has been found to perform better in North America than the earlier MERRA version for precipitation, and snow amounts in particular have been found to have a lower bias and better correlation to reference data in neighboring parts of Canada [*Reichle et al.*, 2017]. Altogether, these findings encouraged our choice of this product as model forcing.

We compare the product to observational meteorological records within our domain and discuss the outcomes in Section 4.

3.3 Model calibration datasets

To help constrain our estimates of glacier mass change and freshwater runoff for the Juneau icefield, we use multiple calibration datasets including: a geodetic glacier mass balance estimate, streamflow measurements, snow water equivalent observations, and ablation observations.

Table 1. Characteristics of gauged watersheds included in calibration routine.

River	Area (km^2)	Glacier cover (%)	Elevation range (m a.s.l.)	Distance between glacier outflow and gauge	Gauge data availability
Mendenhall River	223	56	20 to 1980	5 km with large lake	1980 to 1994; 1996 to 2016
Lemon Creek	31	46	280 to 1620	4 km	2002 to 2016
Montana Creek	36	2	20 to 1480	12 km	1980 to 1987; 2000 to 2012
Cowee Creek	111	11	0 to 1700	15 km with small lake	2013 to 2016

3.3.1 Geodetic glacier mass balance

Several studies have derived geodetic bulk volume loss estimates for the Juneau Icefield, including *Larsen et al.* [2007] who estimated -0.62 m w.e. a^{-1} for 1962 to 2000, *Berthier et al.* [2010] who found -0.53 ± 0.15 m w.e. a^{-1} for 1962 to 2006, *Melkonian et al.* [2014] who found -0.13 ± 0.12 m w.e. a^{-1} for 2000 to 2009/2013, and *Berthier et al.* [2018] who estimated -0.68 ± 0.15 m w.e. a^{-1} for 2000 to 2016. Though the *Melkonian et al.* [2014] study initially suggested a slowdown in mass loss, *Berthier et al.* [2018] points to issues in *Melkonian et al.* [2014] related to unknown penetration depths into firn and snow by the Shuttle Radar Topography Mission DEMs used in their calculations. The mass balance result from *Berthier et al.* [2018], calculated from Advanced Spaceborne Thermal Emission and Reflection Radiometer (ASTER) imagery, agrees closely with laser altimetry approaches and is therefore the value we take as the current best estimate overlapping with our study interval.

In our calibration process, we aim to reproduce the mean annual glacier-wide mass balance rate from *Berthier et al.* [2018] for the same spatial domain (i.e. the glacier outline for the Juneau Icefield, which the authors also obtained from the Randolph Glacier Inventory v6.0). Because the early and late ASTER scenes used in *Berthier et al.* [2018] represent mosaics of different acquisition dates, the authors listed their geodetic estimate as generally spanning 2000 to 2016, without citing specific start or end dates. For comparison to the model, we select start and end dates as the beginning and end of the associated water years, i.e. Oct. 1, 2000 and Sept. 30, 2016.

3.3.2 Streamflow measurements

Semi-continuous time series of discharge data are available for four stream gauges in the Juneau area, including three streams instrumented by the USGS (Mendenhall River, Lemon Creek, and Montana Creek; data available at https://waterdata.usgs.gov/nwis/rt) and one (Cowee Creek) monitored by researchers at the University of Alaska Southeast (Figure 1). Data are available for different time periods for each. The four instrumented basins represent a range of size above the gauge locations, percent glacier cover, elevation range, and distance between glacier outflow and gauge (Table 1). This range of characteristics increases our ability to test model performance across different flow regimes. In our calibration process, we aim to reproduce discharge (Q) from all upstream terrain as routed to the gauge locations.

3.3.3 Snow water equivalent

Point observations of snow water equivalent (SWE) used to drive SnowAssim (Figure 1) are obtained from several published and unpublished sources. All values are converted to SWE following standard glaciological protocols [*Østrem and Brugman*, 1991].

We glean observations for Taku Glacier and Lemon Creek Glacier from *Criscitiello et al.* [2010], and for Mendenhall Glacier from *Motyka et al.* [2002] and *Boyce et al.* [2007]. Additional observations are also available for Taku [*McNeil et al.*, 2019] and Lemon Creek glaciers [*McNeil and O'Neel*, 2019], Taku Glacier (University of Alaska Southeast, Jason Amundsen, unpublished data), and Mendenhall Glacier (University of Alaska Southeast, Mike Hekkers, unpublished data).

During several field campaigns in late April of each 2013, 2014, and 2015, our team also carried out SWE observations at six locations along the Gilkey Glacier centerline between 300 to 1900 m a.s.l., as a means to fill in spatial gaps over the icefield. SWE values were derived using measured density profiles obtained from snow core samples, representing stratigraphic balances. Data are available at *Young* [2019].

Finally, we also incorporate helicopter-borne ground-penetrating radar (GPR) observations collected by USGS along the Taku Glacier and Gilkey Glacier centerlines in spring 2014 and 2015, in collaboration with our field campaigns. Raw GPR data were sourced from *O'Neel et al.* [2018], and were processed by USGS and converted to snow depths using the methods described in *McGrath et al.* [2015]. Density data were sourced from six contemporaneous snow cores measured along each corresponding flight path, where densities were linearly interpolated between locations by the increment $1/n$, where n is the number of ~equally-spaced observations between core sites. By multiplying depths by densities, this dataset is equivalent to ~121,000 and ~39,000 SWE point observations in 2014 and 2015, that we averaged to single annual values within each model grid cell.

3.3.4 Ablation observations

For our calibration routine, we also make use of point snow and ice ablation observations at stake sites from the published and unpublished datasets described in Section 3.3.3. We also leverage melt data from own field campaigns in 2013 to 2015, available at *Young* [2019]. Snowmelt values were calculated by subtracting the SWE equivalent values between snowpacks at known start and end dates. Ice melt values used exposed stake height changes multiplied by an assumed glacier ice density of 900 kg m^{-3}. All ablation observations are compared to model output extracted for the same location and covering the same time span.

3.4 Calibration approach

To correctly characterize glacier mass change and freshwater discharge, we adopt a two-stage calibration approach. The first stage is automated within SnowModel, and leverages the built-in data assimilation sub-routine SnowAssim. SnowAssim is used to compile and interpolate all available ground-based and remotely sensed snow water equivalent data [*Liston and Hiemstra*, 2008]. SnowAssim is run prior to regular SnowModel simulations using a scheme that optimizes interpolation by calculating the differences between observed and modeled snow values and retroactively applies multiplicative corrections to melt factors or precipitation values to create improved fields prior to the assimilated observations. SnowModel is then run again using the new precipitation fields as input. This early, automated form of calibration improves simulations of snow distribution throughout the season rather than only at the time of observation, generating more accurate spatial distribution of snow depth and SWE.

For the second calibration stage, we adopt a traditional grid search approach to tuning model parameters, beginning with a broad search across the parameter space then focusing in on narrower ranges with a finer grid. For this, we identify which of the SnowModel-HydroFlow parameters to treat as tuning parameters and which can be prescribed. SnowModel-HydroFlow has an extensive suite of parameters, many of which have been determined from field measurements or from modeling experiments. Based on a review of other SnowModel-

HydroFlow studies and focusing on importance to localized meteorological and hydrological conditions in glacierized mountain terrain, we initially select seven parameters: glacier albedo, fresh snow albedo, melting (non-forested) snow albedo, monthly precipitation lapse rates, monthly temperature lapse rates, and factors for modifying each the slow and fast reservoir velocities in the HydroFlow routing module (acting to increase or decrease fluid residence time). Preliminary simulations indicate that model results are relatively insensitive to values of fresh snow albedo and the factor for slow reservoir velocities. We therefore focus our calibration efforts on the remaining five parameters. We identify a range of physically realistic values to test for each, as guided by the literature and other SnowModel studies (Table 2). All other SnowModel parameters are set to default SnowModel values, a select list of which is also shown in Table 2.

We next establish calibration datasets and appropriate metrics to evaluate model performance. We first prioritize achieving a match between our estimated SnowModel glacier mass change and the long-term geodetic estimate from *Berthier et al.* [2018]. We aim to minimize the difference between our model results and that derived by *Berthier et al.* [2018] over the same time period. To do this we define $\dot{B}_{\text{diff}}$ as $|\dot{B}_{\text{mod}}$ - $\dot{B}_{\text{geo}}|$ where $\dot{B}_{\text{mod}}$ is the annually-averaged glacier-wide mass change rate from the model and $\dot{B}_{\text{geo}}$ is -0.68 ± 0.15 m w.e. a^{-1}. We next compare HydroFlow output of discharge (Q) to streamflow data for the four local drainages, aiming to obtain Nash-Sutcliffe Efficiency (NSE) [*Nash and Sutcliffe*, 1970] nearest to 1. We generate separate statistics for each instrumented basin, but prioritize matching those with the highest percent glacier cover (Mendenhall River, 56%, and Lemon Creek, 46%). Finally, we also compare output to point observations of snow and ice melt from the field, aiming to minimize RMSE and maximize r^2 values. However, after the initial automated calibration step (SnowAssim) that uses SWE observations to determine melt factors, modeled point melt values are relatively insensitive to parameter value change, indicating that the melt factors derived from SnowAssim produce an optimized modeled to observed match.

In summary, we prioritize our performance metrics in the following order: 1) $\dot{B}_{\text{diff}}$ = $|\dot{B}_{\text{mod}}$ - $\dot{B}_{\text{geo}}|$ nearest to 0 for glacier-wide mass balance rates; 2) NSE nearest to 1 for streamflow discharge, prioritizing the statistics for more glacierized basins first; 3) minimizing RMSE and maximizing r^2 statistics for point melt observations. While this focus ensures that we reproduce the glacier component of the overall water balance well, we find that it means sacrificing goodness-of-fit to stream gauge measurements in basins with less glacier cover (Montana Creek, 2%, and Cowee Creek, 11%). We accept this a cost of striving to correctly characterize glacier volume change and glacier runoff production, which are the focus of our study.

For our final time series analysis, we identify out of our 215 simulations all those that generate glacier mass balance estimates for the full icefield that fall within the error bounds of the $\dot{B}_{\text{geo}}$ goal value for Oct. 1, 2000 to Sept. 30, 2016. This yields an ensemble among which is a midpoint ensemble member that most closely matches the goal value, i.e. with $\dot{B}_{\text{diff}}$ = 0, as well as two ensemble end members whose mass balance rates correspond to the upper and lower limit of the *Berthier et al.* [2018] estimate error bars. We use these end members as upper and lower estimates of uncertainty for our midpoint simulation, which we focus on for the bulk of our analyses.

3.5 Model validation

To independently validate our model results, we utilize a time series of terrestrial water changes for the Juneau Icefield area derived from the independent data source GRACE.

Table 2. Calibration parameters for SnowModel-HydroFlow simulations. Note that we also list a selection of prescribed parameters that are not varied.

Parameter	Description and units	Range of values tested	Basis in the literature for tested range	Final value ensemble range and (**best**)
α_{i}	Glacier ice albedo	0.05 to 0.65	0.3 to 0.65 recommended in *Cuffey and Paterson* [2010] for clean to blue ice based on literature; lower limit also extended	0.30 to 0.40 **(0.30)**
α_{smc}	Melting non-forested (clearing) snow albedo	0.15 to 0.70	Although the recommended range for old wet snow is 0.3 to 0.7 in *Cuffey and Paterson* [2010]; we extend the lower limit to account for dust, black carbon [*Nagorski et al.*, 2019] and snow algae [*Ganey et al.*, 2017])	0.40 to 0.50 **(0.50)**
α_{smf}	Melting forested snow albedo	–	Default SnowModel value, and same as *Beamer et al.* [2016], which found model results for the Gulf of Alaska to be relatively insensitive to this value	0.45
α_{sf}	Fresh snow albedo	–	Model results insensitive on initial tests	0.75
$\Gamma_{\mathrm{Jan}}, \Gamma_{\mathrm{Feb}}$ ...	Monthly varying temperature lapse rates (showing Jan/June in °C km^{-1})	2.4/6.2 to 6.4/10.2	We test the SnowModel default seasonal pattern and modify in ± 0.5°C km^{-1} steps	2.4/6.2 to 4.4/8.2 **(3.9/7.7)**
$\chi_{\mathrm{Jan}}, \chi_{\mathrm{Feb}}$ ...	Monthly varying precipitation lapse rates (showing Jan/June in km^{-1})	0.20/0.05 to 0.50/0.35	We test the SnowModel default seasonal pattern and modify in ± 0.5 km^{-1} steps	0.20/0.05 to 0.35/0.20 **(0.20/0.05)**
$\mathrm{f_f}$	Factor for fast response time; channel flow	0.05 to 2.0	Recommended range in HydroFlow	0.25 (**0.25**)
$\mathrm{f_s}$	Factor for slow response time; matrix flow	–	Model results insensitive on initial tests; value same as *Beamer et al.* [2016]	0.05
$\mathrm{T_{rain}}, \mathrm{T_{snow}}$	Threshold rain/snow temperatures (°C)	–	Default SnowModel values, common in modeling studies, e.g. *Young et al.* [2018], *Beamer et al.* [2016]; *Rohrer* [1989]	0/2

3.5.1 GRACE gravimetry data

On account of their substantial magnitudes, both long-term and seasonal terrestrial mass variations from glacier ice loss and snow loading along the Gulf of Alaska are large enough to alter local gravity fields. The GRACE satellites, whose mission lasted from 2003 to 2016, were tandem satellites that used a microwave K-band inter-satellite ranging system to measure gravity changes of all Earth system components. GRACE processing involves forward-modeling of gravity signals from glacial isostatic adjustments, Earth tides, ocean tides, and atmospheric loading (i.e. clouds) in order to isolate the remaining signal of interest [*Wouters et al.*, 2014].

To independently validate our model results, we choose GRACE data from NASA Goddard Space Flight Center Geodesy Laboratory's high resolution v2.4 mass concentration (mascon, i.e. grid cell) solution, which provides mass change estimates at ~30-day intervals and 1° x 1° (~12,390 km^2) resolution [*Luthcke et al.*, 2013]. Data are available at https://earth.gsfc.nasa.gov/geo/data/grace-mascons. This solution represents the full terrestrial water budget – i.e. snowfall, rain, and runoff from nonglacierized and glacierized terrain, including glacier ice melt – and is therefore optimized for terrestrial hydrology. We focus on the two GRACE mascons containing the Juneau Icefield (Figure 1). We choose this GRACE product because it is one of few that explicitly corrects for local mass increases from post-Little Ice Age disintegration of the Glacier Bay icefield [*Larsen et al.*, 2005], as estimated using the ICE-5G glacial isostatic adjustment model [*Peltier*, 2004]. This GRACE product also compares well with regional-scale mass balance model simulations for the Gulf of Alaska [*Hill et al.*, 2015; *Beamer et al.*, 2016] and to mass loss estimates from NASA's Ice, Cloud, and Land Elevation Satellite (ICESat) [*Arendt et al.*, 2013]. Moreover, this solution is among the first to provide information for constructing 95% confidence intervals on mass changes for individual mascons based on estimates of noise and leakage, as detailed in *Loomis et al.* [2019].

The primary benefit of using GRACE data is the high temporal resolution which provides water balance information at sub-annual timescales. Additionally, GRACE provides a direct measurement of mass changes; that is, no density assumptions are required to estimate snow and ice mass loss, which are a large source of uncertainty in other water and glacier mass balance methods. The disadvantage of GRACE is that the fundamental spatial resolution of the v2.4 processing approach is a 300 km Gaussian smoothing filter [*Luthcke et al.*, 2013], resulting in a) coarse resolution, and b) the possibility of signal leakage across mascon boundaries, a processing artifact.

For comparison of our model results to the GRACE time series, our model spatial domain includes all terrain within the two GRACE mascons surrounding the icefield. We extract this spatial domain and select mass change estimates at dates corresponding with the mid-points of the GRACE time series monthly averages. We calculate the long-term mass loss trend by fitting an annual sinusoid to data using a least-squares approximation. Individual annual amplitudes are calculated by subtracting annual minima from maxima, an approach deemed appropriate for the Gulf of Alaska region due to its clean seasonal signal relative to noise [*Luthcke et al.*, 2013].

3.6 Water balance, glacier mass balance, and runoff calculations

Using SnowModel-Hydroflow as described above, the water balance for our domain is calculated by:

$$\dot{S} = \dot{P} - \dot{R} - \dot{ET} - \dot{SU} \tag{1}$$

where S is the volume of water stored within the seasonal snowpack, glacier ice, or top 1 m of soil; P is precipitation input (rain or snow); R is runoff (defined as the water immediately available for routing to downslope areas); ET is evapotranspiration; and SU is sublimation at the snow surface. Dot notation indicates that all quantities are taken to be rates (time derivatives). Note that because none of the glaciers within the domain are ocean-terminating, we do not include marine iceberg calving or submarine melt within equation (1). Although several glaciers are lake-terminating, previous studies on the Mendenhall Glacier (historically land-terminating but now ending in a proglacial lake) revealed that iceberg calving represents only 4 to 6% the amount of ice lost through surface melt [*Boyce et al.*, 2007; *Motyka et al.*, 2002]. Similar to *Ziemen et al.* [2016], we therefore consider ice discharge into lakes to be a small component of Juneau Icefield glacier mass balance, and an even smaller part of water balance of the coastal watershed.

In SnowModel, runoff R is water that is immediately available to be routed downstream, and is the sum of glacier ice melt, snowmelt that does not refreeze or fill pore space within the snowpack, rain on bare surfaces (i.e. rain that does not fall onto snow or soil substrates), or rain on already-saturated snow or soil. We note that the term 'glacier runoff' is used ambiguously within the literature and often represents different physical quantities [*O'Neel et al.*, 2014; *Radić and Hock*, 2014]. For our purposes, we define glacier runoff as all runoff produced over glacierized cells. This formulation is identical to two studies that modeled runoff for the Gulf of Alaska [*Beamer et al.*, 2016; *Neal et al.*, 2010] as well as to the quantity defined conceptually in *O'Neel et al.* [2014] as total runoff from the glacier surface (concept 5). We use the term 'glacier ice melt' separately, to denote meltwater from the glacier surface only after snow cover has been removed (i.e. it is one component of glacier runoff). We calculate both quantities throughout the study.

We calculate the area-averaged glacier mass balance using equation (1) over glacierized grid cells only (noting that evapotransporation (ET) goes to zero over glacier surfaces). Glacier mass balance therefore represents a portion of the full spatial domain's water storage S. The contribution of non-glacierized cells makes up the remaining portion.

All comparisons of model output to stream gauge instruments are comparisons to:

$$Q = \dot{R} - \dot{ET} \tag{2}$$

i.e. discharge Q (a flux) is all runoff that has been routed to a known gauge location, after evapotransporation ET has been taken into account.

Finally, comparisons of model output to GRACE data are to water storage S, given that the GRACE satellites measure all changes in water mass distribution over Earth's surface.

3.7 Trend analyses

We evaluate trends in magnitude and timing of hydrological variables (total runoff, glacier runoff, glacier ice melt, and water balance), integrated over the full spatial domain draining west to the coast. For trends in magnitude, we examine spatially and temporally integrated quantities including annual volumes of total runoff, precipitation, glacier runoff (the sum of ice melt, snowmelt, and rain on the glacier surface), glacier ice melt (i.e. melt at the glacier surface after snow has been removed), and water balance. We also identify maximum and minimum daily values for each year for total runoff, glacier runoff, glacier ice melt, and water balance. Further, we examine volumes of glacier runoff and ice melt for spring and summer seasons, where each season's start and end dates are defined by the maximum, minimum, and inflection points of the domain- and temporally-averaged annual air temperature climatology derived from the MicroMet-interpolated climate input data. Here, 'winter' falls between December 24 to April 6, 'spring' is April 7 to July 17, 'summer' is July 18 to October 11, and 'fall' is October 12 to Dec 23. Finally, we assess cold season volumes of glacier runoff and glacier ice melt. Here, the cold season is defined as the period between late-fall termination and spring onset of glacier runoff and ice melt, which correspond to the latest and earliest dates that respectively follow or precede a period of at least two weeks of glacier runoff/ice melt below a near-zero threshold. This two-week criteria was chosen out of several algorithms for best reproducing manually-selected dates.

For trends in timing, we use the raw complete time series to test for trends in: day of year of minimum daily volumes of total runoff and water balance; day of year of glacier runoff and glacier ice melt onset and end, as well as the length of the season in between; and number of non-zero days of cold season glacier runoff and ice melt. For trends in the timing of peak flows (i.e. maximum daily volumes of total runoff, water balance, glacier runoff, and glacier ice melt) in particular, we test for day of year trends in a time series smoothed with a 14-day running mean in order to capture the overall shape of the hydrograph and minimize the effect of extremes.

Trends are detected using the Mann-Kendall test for significance, a non-parametric test (i.e. data do not have to meet the assumption of normality). Trends are calculated using the Theil-Sen estimator, a non-parametric approach that fits a trend by determining the median of the slopes of lines through each pair of points in a sample. This approach is more robust against outliers than simple linear regression, making it well-suited to, and commonly used in, hydrological applications [*Helsel and Hirsch*, 2002]. To identify the statistical significance of each trend, we report a harmonic mean p-value, a formulation for combining p-values from tests that cannot be guaranteed to be independent [*Wilson*, 2019], e.g. model simulations with the same input data and physics but variation in parameter values. We calculate a harmonic mean p-value for every trend by equally weighing our midpoint and two end member simulation p-values.

In reporting our findings, we take an approach that extends beyond the traditional method of judging results as meaningful solely by the p-value ≤ 0.05 criteria. This has been challenged in recent years, citing limitations such as variation in p-value statistics across replicate studies [*Halsey et al.*, 2015] and difficulty in interpreting results when the p-value is high and the null hypothesis cannot be rejected [*Cohen*, 2016]. We turn instead to recommendations from *Halsey* [2019] and *Tomczak and Tomczak* [2014] to include in our analysis a measure of effect size (which in our case is the trend itself) as well as 95% confidence intervals surrounding that trend, in order to provide additional insight into the range of possibilities that are reasonably likely. We also heed advice from *Amrhein et al.* [2019] that including factors such as background evidence, data quality, and understanding of underlying mechanisms can contribute to meaningful interpretation of statistical results. As such, we include as an interpretive tool for the reader a qualitative assessment of our confidence that a positive trend should be detected, in the context of our full suite of results and a priori current knowledge from the literature for each climatological and hydrological variable.

4 Model initialization and calibration

In this section, we describe outcomes from the initialization and calibration process, from which we are better able to understand the strengths and limitations of our model results.

To assess the performance of the MicroMet meteorological interpolation module, we compare daily MicroMet-interpolated MERRA-2 air temperature fields to observations from National Oceanic and Atmospheric Administration (NOAA) airport weather stations at Juneau and Skagway (Figure 1), and find strong correlation (r^2 = 0.92 and 0.88, respectively). However, we find systematic biases between modeled and observed temperatures, when averaged monthly, with lower than observed temperatures in winter months (as large as of -2.1 °C in Juneau and -5.5 °C in Skagway) and higher than observed temperatures in summer months (as large as 2.0 °C in Juneau and 2.8 °C in Skagway). In terms of daily precipitation, modeled and observed volumes were weakly correlated in both Juneau (r^2 = 0.52) and Skagway (r^2 = 0.40). Mean monthly modeled fields also overproduced precip-

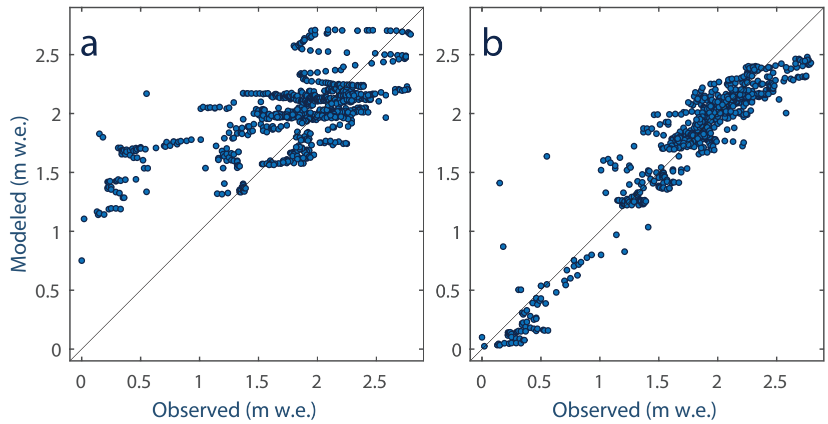

Figure 2. Comparison of observed versus modeled snow water equivalent (SWE) values at on-glacier locations both a) before, and b) after the application of the SnowAssim initial calibration routine. Results are shown for the ensemble member driven with the best fit parameters; other ensemble members are similar.

itation, particularly in fall and early winter months, with biases between 1.3 and 4.7 mm w.e. d^{-1} for Juneau and 0.8 to 2.3 mm w.e. d^{-1} for Skagway. Note that we did not apply a monthly bias correction to the model fields for temperature or precipitation because both weather stations used for comparison are biased to low elevations, and we have no additional information for spatially distributing a correction across the large distance and complex topography between the airports. We assume, therefore, that these biases are accommodated for by adjustment to the tuning parameter suite.

We evaluate the impact of our initial calibration routine SnowAssim by comparing SnowModel on-glacier point SWE estimates to observations from glacier mass balance field and airborne campaigns (Figure 2). We observe that model reproduction improved markedly from r^2 = 0.45 to r^2 = 0.90 and RMSE = 0.45 m w.e. to RMSE = 0.18 m w.e (Figure 2). This highlights that the SnowAssim routine produces more realistic SWE fields irrespective of location or duration between observations. The model also reproduces independent point melt (i.e. snow/ice ablation) observations, with r^2 = 0.79 and RMSE = 1.63 m w.e (Figure 3). The larger RMSE values are not unexpected given the predominance of ablation measurements at lower elevations in the ablation area (60% of the observations are at < 800 m a.s.l.), which on large glaciers with undulating surface topography often display substantial local variability that may not be well-captured by the model (e.g. *Young et al.* [2018]). However, we note that the model appears to underpredict melt for more negative point mass balances, which may be due to the above-mentioned lower-than-observed temperatures in the summer months.

In the second calibration phase, we succeed in tuning parameters to reproduce the geodetic mass balance rate from *Berthier et al.* [2018], -0.68 ± 0.15 m w.e. a^{-1} for 2000 to 2016. From the ensemble of all simulations that meet this criteria, we focus our primary analysis on the midpoint simulation with a mass balance rate of exactly -0.68 m w.e. a^{-1}, and consider the ensemble end members – whose mass balance rates are nearest the upper and lower error bounds from *Berthier et al.* [2018] – to be the limits of our uncertainty. Best-fit parameter values are shown in Table 2. This step of calibrating to a long-term mass balance rate is crucial for correctly characterizing glacio-hydrological systems. Had we not undertaken this step, our initial simulations using SnowModel default parameter values would have yielded a mass balance rate of +0.08 m w.e. a^{-1}.

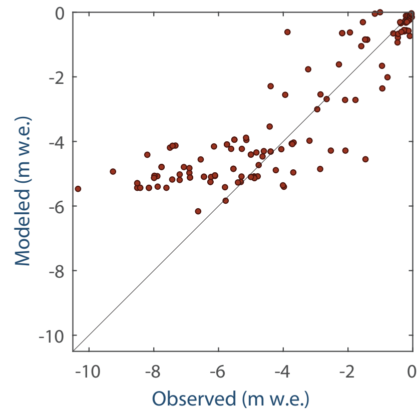

Figure 3. Comparison of observed versus modeled point snow/ice ablation values at on-glacier locations, as driven with the best fit parameters.

Our ability to reproduce observations from stream gauge records on the four instrumented basins varies by the amount of glacier cover (see Figure 4). For the two glacierized basins with the largest percent cover, comparison of modeled to observed monthly discharge yields stronger agreement: for Mendenhall River (56% glacier cover), we obtain NSE = 0.84 and r^2 = 0.88, and for Lemon Creek (46% glacier cover), we find NSE = 0.76 and r^2 = 0.82. The model, however, is unable to reproduce many of the large peaks in the daily Mendenhall discharge record, several of which are associated with recent (2011 and on) glacier lake outburst floods from an upstream tributary basin. The model does not include a mechanism to generate these impulsive events. For the two basins that are predominantly forested, modeled to observed agreement is weaker: for Montana Creek (2% glacier cover), we find NSE = -1.37 and r^2 = 0.45, and for Cowee Creek (11% glacier cover), we obtain NSE = -0.81 and r^2 = 0.47. We also note that the Mendenhall River and Lemon Creek watersheds show evidence of seasonal biases between modeled and observed quantities, with the model generally over-producing runoff in summer and under-producing in fall. We discuss this, and provide possible reasons for the modeled-to-observed discrepancy in less-glacierized basins, in Section 6.1. Altogether, weighing all four basins according to both above-gauge basin area as well as length of observational record, we calculate a weighted NSE = 0.21 and weighted r^2 = 0.73. We believe this performance to be acceptable given that, rather than any one process in isolation, streamflow represents an integration of all glacio-hydrological processes in the watershed, and thereby has the potential to integrate any sources of error with input data as well as model physics into a single metric. Because our model performs well in reproducing other calibration datasets, particularly in glacierized watersheds (e.g. our estimate for the 2000 to 2016 mass balance rate for the Mendenhall Glacier alone is -0.73 m w.e. a^{-1}, which matches the estimate of -0.73 ± 0.13 m w.e. a^{-1} from *Berthier et al.* [2018]), we are confident in the calibrated model performance.

5 Results

5.1 Glacier mass balance

Our modeled, tuned annual glacier-wide mass balance rate for the Juneau Icefield is -0.68 m w.e. a^{-1} for 2000 to 2016, with lower and upper uncertainty bounds of -0.57 and -0.83 m w.e. a^{-1} corresponding to our simulation ensemble end members. Extending to the full model period of Oct. 1, 1980 to Sept. 30, 2016, we calculate a rate of -0.57 [-0.11, +0.12] m w.e. a^{-1} for the icefield, suggesting an acceleration in recent decades. Fi-

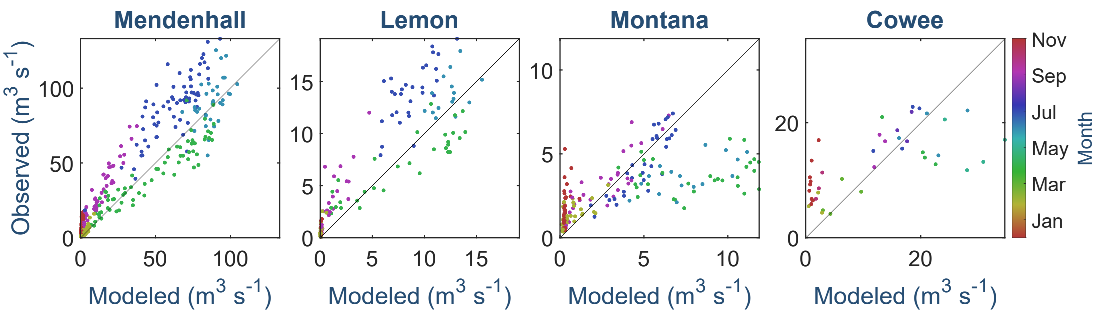

Figure 4. Mean monthly discharge Q from observations versus model results for four instrumented watersheds in cubic meters per second, as driven with the best fit parameters. Note the differing axis scales.

nally, for all ice contained within the domain draining to the coast, our model estimates a mass balance rate of -0.81 [-0.08, +0.11] m w.e. a^{-1} for 1980 to 2016, suggesting that the ice nearest the coast (i.e. to the west of the topographic divide) experiences greater rates of mass loss than the more interior glaciers. Cumulative glacier-wide specific mass balance for the full model period is shown in Figure 5. Annual glacier mass balance over this time period and domain is comprised of, on average, 3.07 ± 0.01 m w.e. a^{-1} of precipitation, 3.85 [-0.08, +0.10] m w.e. a^{-1} of glacier runoff, and 0.03 ± 0.01 m w.e. a^{-1} of sublimation from the snow surface.

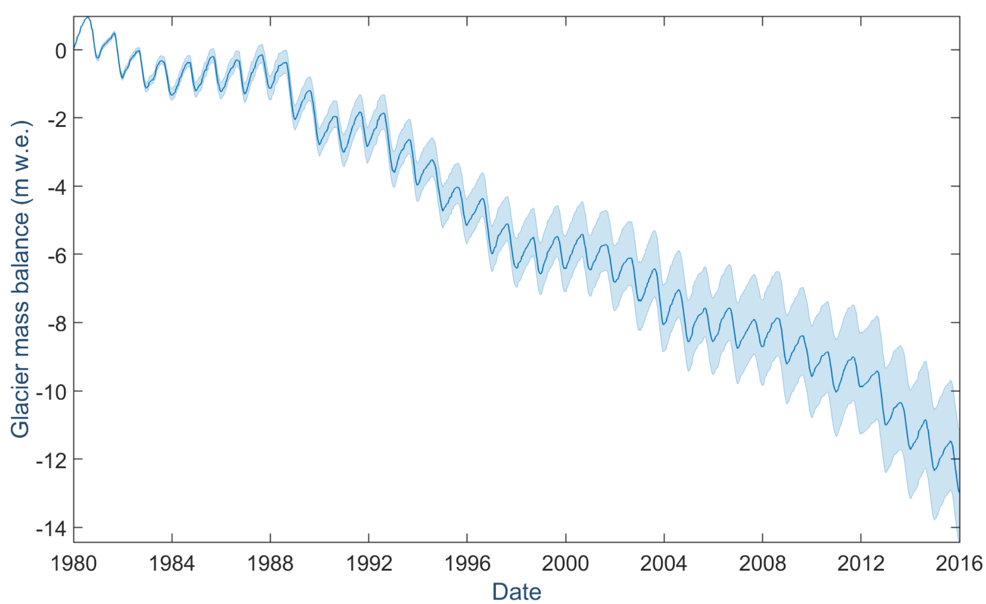

Figure 5. Modeled cumulative glacier-wide specific mass balance for the full model period of Oct. 1, 1980 to Sept. 30, 2016 for all coastal ice of the Juneau Icefield. The upper and lower limits of uncertainty correspond to the model ensemble end members, whose trends correspond to the upper and lower limits of uncertainty of the calibrating geodetic mass balance estimate for 2000 to 2016 from [*Berthier et al.*, 2018].

5.2 Freshwater runoff

For the watershed encompassing all Juneau Icefield glacier ice draining to the coast, we estimate mean annual freshwater runoff of 20.0 [+0.5, -0.4] km^3 a^{-1} for 1980 to 2016. Of this, 11.0 ± 0.3 km^3 a^{-1} (or 55 ± 1%) is glacier runoff (i.e. runoff sourced from the glacier surface). The water balance volume we calculate is, on average, -2.1 [+0.4, -0.3] km^3 a^{-1}, though as we discuss below in Section 6.1 this is believed to be an underestimate of the long-term water storage loss. For ice-only cells, we calculate water storage losses (i.e. glacier volume loss) of 2.4 [-0.3, +0.2] km^3 a^{-1} for the same time period, which means that glacier volume loss (the percentage of runoff due to the persistent negative mass balance trend, rather than seasonal magnitudes of glacier runoff) comprises 12 ± 1% of total runoff in the domain and 22 [+1.0, -1.4] % of glacier runoff. Precipitation over the full domain delivers an average of 18.3 km^3 a^{-1}, while evapotranspiration and sublimation from the snow surface are small, at 0.17 [-0.07, +0.02] km^3 a^{-1} and 0.17 [-0.07, +0.02] km^3 a^{-1}. Mean monthly values of each of these variables are shown in Figure 6, though evapotranspiration and sublimation are not visible at this scale.

To better understand the linkages between individual water balance components, we assess the correlation between different modeled quantities. We find that annual volumes of glacier runoff and total runoff for the domain are highly correlated (r^2 = 0.90, $p <$ 0.001), while glacier runoff and glacier ice melt are less so (r^2 = 0.68, $p < 0.001$). Glacier ice melt is also weakly correlated with total runoff (r^2 = 0.45, $p < 0.001$).

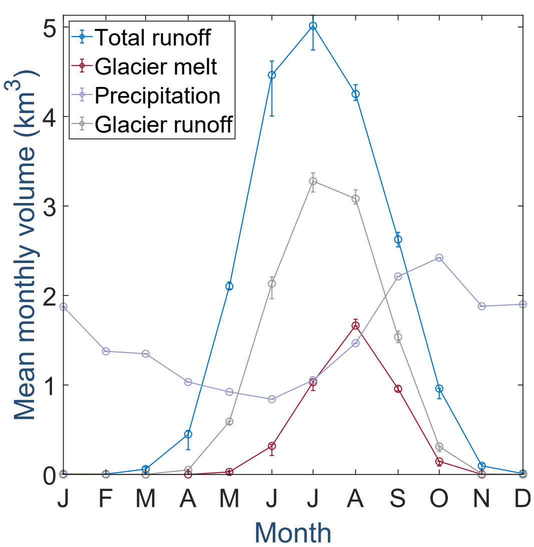

Figure 6. Mean monthly volumes of total runoff, glacier runoff, glacier ice melt, and precipitation for the full 1980 to 2016 period. Note that evapotranspiration and sublimation, though included within our model calculations, are very small and not shown.

5.3 Water balance and comparison with GRACE

For the 2003 to 2016 period overlapping with GRACE data availability, we calculate a glacier-wide mass balance rate for all ice in the GRACE two-mascon domain of -0.51 [-0.18, +0.13] m w.e. a^{-1} (or -2.5 [-0.9, +0.6] km^3 a^{-1}), in close agreement with the GRACE-derived negative trend estimate of -0.55 m w.e. a^{-1} (-2.7 km^3 a^{-1}), as shown in Figure 7a. Correlation between these two time series is robust, with r^2 = 0.91 and $p <$ 0.001 (Figure 7b). These results showcase the model's ability to reproduce the climatic conditions over the ice-covered portions of the domain that are driving sub- and interannual water storage changes.

However, in comparing GRACE to modeled results for ice and land cells together, we observe that correlation is less strong (r^2 = 0.36, $p < 0.001$). This discrepancy can be seen in the SnowModel land+ice time series in Figure 7a primarily as a lack of agreement in the overall trend, which is not sufficiently negative at -0.002 m w.e. a^{-1}. We discuss this further in Section 6.1. Nonetheless, our full SnowModel land+ice water balance produces seasonal amplitudes (mean annual accumulation = 25.8 km^3 a^{-1}, ablation = -26.6 km^3 a^{-1}) that are more in line with those from GRACE (18.1 and -21.5 km^3 a^{-1}) than those from ice cells alone (9.0 and -12.1 km^3 a^{-1}). This result is encouraging as, again, the GRACE solution we use measures all components of the terrestrial water balance.

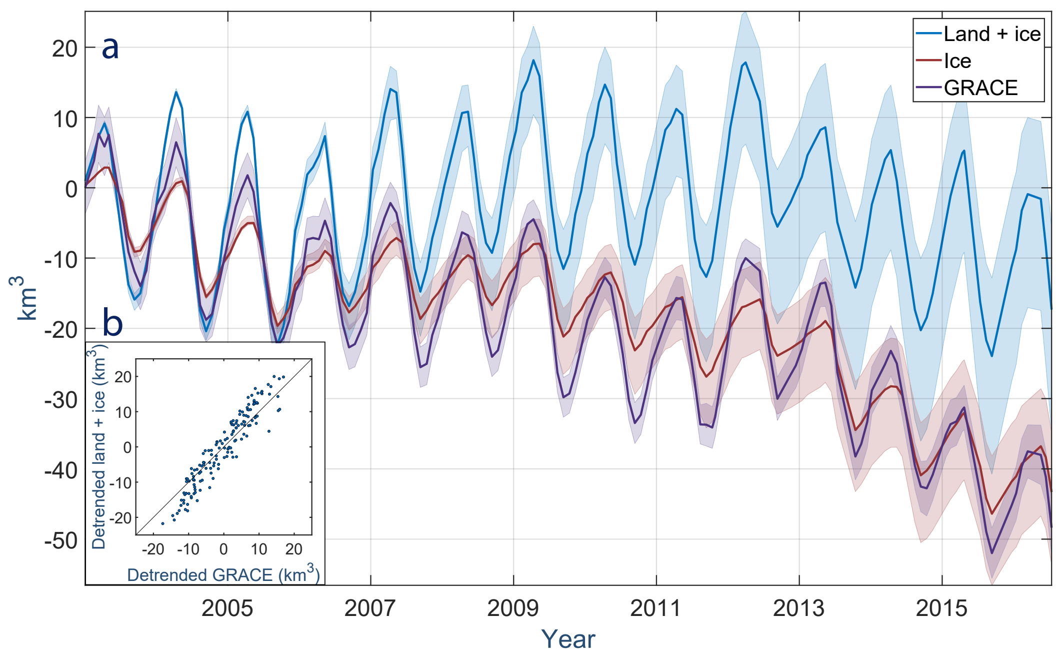

Figure 7. a) Water balance time series comparing the GRACE two-mascon domain for 2003 to 2016 (purple) with that derived from SnowModel with land+ice cells together (blue) and ice cells only (red). b) Scatter plot comparison of detrended modeled land+ice water balance values versus equivalent from GRACE.

5.4 Trends in magnitude and timing

We next assess trends in the timing and magnitude of different hydrological variables, and summarize results of trend detection tests in Table 3. In the spirit of reports from the International Panel on Climate Change (e.g. *Masson-Delmotte et al.* [2018]), we also include as an interpretive guide a column with a qualitative assessment of our confidence that a positive trend should indeed be present in each specific variable, given the trend result in context with our full suite of results as well as a priori information.

To help interpret our model output results, we first assess trends in the principal input variables of precipitation and mean air temperature. We find no reliable trend in annual precipitation volume, but do find an increase in mean air temperature (0.1 °C per decade), which is consistent with recent analyses of air temperature trends in Alaska, including *Bieniek et al.* [2014] who found a 0.2 °C increase in the northern portion of the Juneau Icefield between 1980 to 2012.

Of all variables tested, the most statistically robust ($p \leq 0.05$) trends are related to shifts in timing of the peaks of the 14-day smoothed glacier ice melt curve (occurring 2.5 days earlier per decade) and glacier runoff curve (occurring 4.4 days later per decade) (Figure 8). The day of year of the water balance minimum is also found to be occurring 3.5 days earlier per decade.

From a seasonal perspective, the most statistically robust trends with the largest effect sizes occur in our hydrological variables in the spring season (Figure 9). We also observe an increase in glacier ice melt in summer.

Among the different hydrological variables examined, the most robust trends are related to glacier ice melt. These include the volume of spring glacier ice melt (increasing by 16.5% per decade) and, with slightly less statistical strength, the annual volume of glacier ice melt (9.6% per decade), both of which are visible in Figure 10. Our results also suggest an increase in the magnitude of the maximum daily volume of glacier ice melt (10.2% per decade).

The large degree of interannual variability in precipitation in this domain increasingly acts to obscure trend detection as the proportion of non-glacier ice grid cells grows in a particular hydrological variable (Figure 10). In other words, when examining volumes, we observe the pattern that trends for glacier ice melt, glacier runoff, and total runoff exhibit respectively smaller proportion change with less robust statistical significance. For example, in spring months, we calculate p-values of 0.05, 0.11, and 0.25, and respective trends of 16.5, 6.8, and 2.7% per decade for those three variables. This pattern holds true for each spring, summer (not shown in table), and annual periods, and disappears during fall and winter months when glacier ice melt ceases almost entirely.

Finally, our results also suggest trends for variables associated with colder months, including an increase in the number of days of non-zero glacier runoff during the cold season (2.4 days per decade), but a decrease in the volume of glacier runoff during winter months (-5.8% per decade).

To visualize some of these changes spatially, Figure 11 shows both the mean annual spatial distributions of freshwater variables for 1980 to 2016 throughout the coastal domain, as well as anomalies from these mean values for the years 1980 to 1990 and 2010 to 2016. These panels demonstrate a significant shift in spatially distributed volumes of freshwater from the beginning and end periods of our model interval.

Of the remaining variables tested, none show trends we believe to be reliable according to our methods, although some may prove to be significant in future years. Of these, fall season volumes show the lowest p-values of any season for all hydrological variables, followed by the winter season. Maximum and minimum daily volumes do not exhibit changes in either volume or timing. Volumes of cold season glacier ice melt and glacier runoff do not appear to have changed substantially over the period of study, nor does the frequency of cold season glacier ice melt events. Finally, we do not detect reliable trends in the onset and end of glacier ice melt or glacier runoff, nor in the length of the melt season in between, although future analyses may reveal changes to these.

6 Discussion

6.1 Model performance

Overall, our model calibration approach achieves robust agreement with calibrating datasets of snow water equivalent point mass balance, long-term geodetic glacier-wide mass balance, snow and ice melt point mass balance, and discharge in highly glacierized basins. These results highlight our ability to effectively combine the suite of different

Table 3. Results of trend detection tests for select hydrological variables for all terrain draining west from the Juneau Icefield to the coast. Here all variables are defined as positive (e.g. glacier ice melt is positive even though it represents a loss), such that positive/negative trends correspond to increasing/decreasing quantities in all cases. p-values are given by the harmonic mean of individual Mann-Kendall tests for the midpoint, upper, and lower end member simulations, and **bold** indicates the trends that are statistically strongest. Trends are given by the Theil-Sen slope and a 95% confidence interval is provided for each. The percent change per decade is indicated for the mean trend (column 3) relative to the 1980 to 1989 period. Finally, the last column shows our qualitative assessment of confidence that a positive trend should be present, given our results and in context with the literature (VC = very confident, C = confident, SC = somewhat confident, NC = not confident).

Variable	p-value	Trend and units (a^{-1})	95% confidence interval	% change $(\mathrm{decade})^{-1}$	Trend confidence
Input variables:					
Mean annual air temperature	0.27	0.01 °C	[0.00, 0.06]	–	VC
Annual precipitation volume	0.75	-1.7e7 m^3	[-1.2e8, 5.5e7]	-0.9	NC
Mean spring air temperature	0.19	0.03 °C	[0.02, 0.09]	–	VC
Spring precipitation volume	0.87	-2.2e6 m^3	[-2.9e7, 1.9e7]	-0.7	NC
Winter precipitation volume	0.10	-3.3e7 m^3	[-2.1e7, 1.9e7]	-1.3	NC
Model output:					
Annual runoff volume	0.48	2.8e7 m^3	[-2.0e7, 1.4e8]	1.4	SC
Annual glacier runoff volume	0.23	3.1e7 m^3	[8.1e6, 1.3e8]	3.0	C
Annual glacier ice melt volume	0.14	3.6e7 m^3	[2.0e7, 1.2e8]	9.6	VC
Spring runoff volume	0.25	2.5e7 m^3	[4.6e6, 8.8e7]	2.7	C
Spring glacier runoff volume	0.11	2.7e7 m^3	[1.8e7, 8.8e7]	6.8	VC
Spring glacier ice melt volume	**0.05**	1.0e7 m^3	[1.0e7, 3.2e7]	16.5	VC
Summer glacier ice melt volume	0.18	2.5e7 m^3	[8.2e6, 8.3e7]	1.8	C
Winter glacier runoff volume	0.16	-4.9e4 m^3	[-2.0e5, -4.8e4]	-5.8	SC
Max daily glacier ice melt	0.12	2.0e3 m^3	[1.6e3, 6.7e3]	10.2	C
DOY of min water balance	0.09	-0.35 days	[-1.2, -0.26]	–	VC
No. of cold season glacier runoff days	0.19	0.24 days	[0.20, 0.86]	25.8	C
DOY of smoothed glacier runoff peak	**0.05**	0.44 days	[0.39, 1.29]	–	C
DOY of smoothed glacier ice melt peak	**0.04**	-0.25 days	[-0.78, -0.25]	–	VC

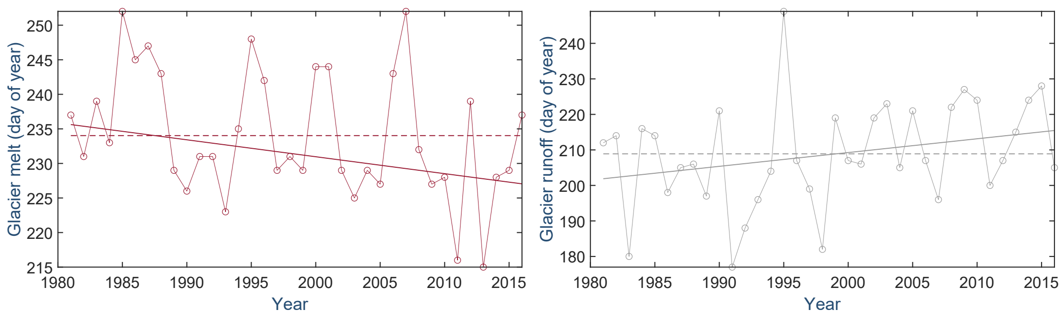

Figure 8. Timing of smoothed annual peak of glacier ice melt and glacier runoff in coastal domain. Each panel shows the time series (circles), mean (dotted line), and trend (solid line).

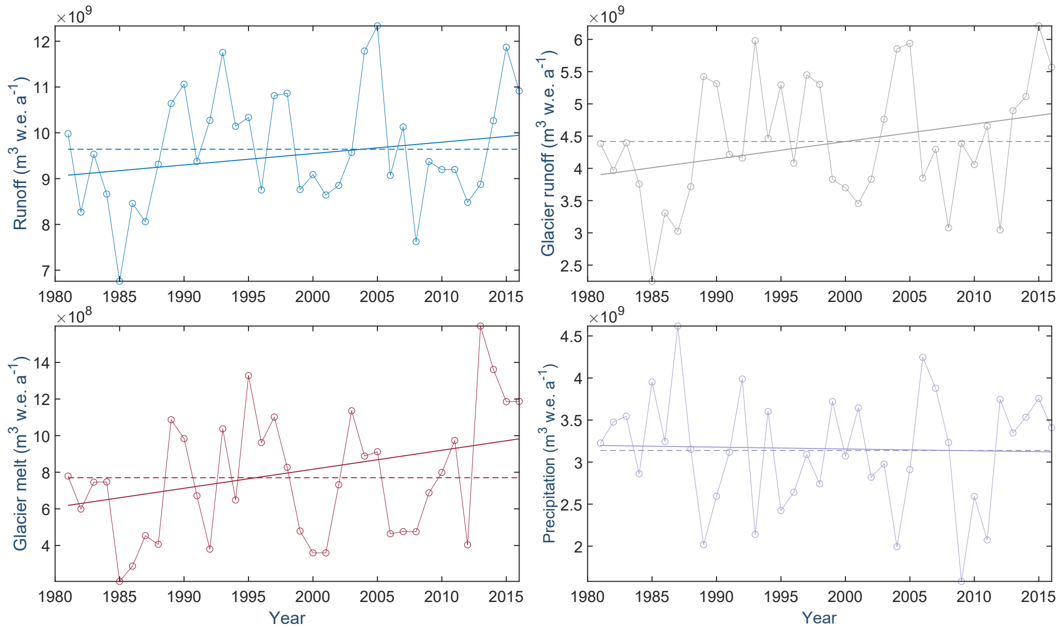

Figure 9. Total runoff, glacier runoff, water balance, and glacier ice melt volumes for spring season in the coastal domain. Each panel shows the time series (circles), mean (dotted line), and trend (solid line).

physically-based sub-models needed to reproduce accumulation, ablation, and hydrological processes in these complex, glacierized basins.

6.1.1 Parameter tuning – system dominated by ice and snow albedo

Glacier ice albedo and melting snow albedo in clearings (i.e. non-forested areas, including over glaciers) prove to be the most important parameters for correctly reproducing glacier mass balance rates on par with those from *Berthier et al.* [2018]. We tune both parameters to values on the low end of typical ranges seen in the literature (i.e. 0.30 to 0.40 for glacier ice albedo and 0.40 to 0.50 for melting snow albedo in clearings). The lower values may be explained by the presence of both snow algae (documented on another coastal icefield in Alaska in *Ganey et al.* [2017], and observed by the first author in the field) as well as dust and black carbon [*Nagorski et al.*, 2019]. Both of these light absorbing impurities contribute to an amplifying feedback process by lowering albedo and increasing melt rates, which in turn consolidates material on the snow surface and fur-

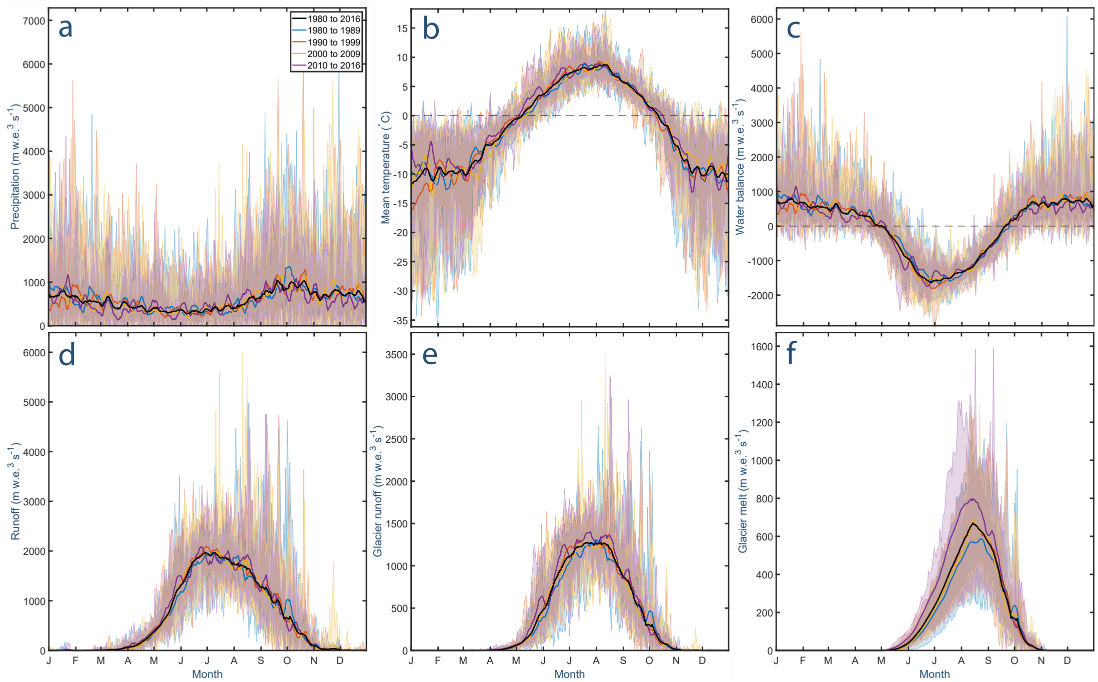

Figure 10. Stacked graphs of modeled output of a) precipitation, b) air temperature, c) water balance, d) total runoff, e) glacier runoff, and f) glacier ice melt for the coastal domain. Solid colored lines represent the daily mean output for each decade, while shaded regions in matching colors represent the corresponding daily range for all years within the given decade. The solid black line shows the 1980 to 2016 mean.

ther increases melt rates. *Nagorski et al.* [2019] confirm through measurement that dust and black carbon density at the surface increases later in the melt season, suggesting that snowpack 'aging' should be taken into consideration in future melt modeling efforts. Incorporating this process by allowing for monthly-varying albedo values would likely improve our SnowModel-HydroFlow simulations of late-summer freshwater discharge by increasing glacier ice melt and snowmelt during those months. Modeled glacier mass balance rates were insensitive to the value of fresh/dry snow albedo, consistent with the fact that the coastal Juneau Icefield is dominated by aged or wet snow during the runoff season.

We find that within the tested range of precipitation lapse rates, those that were the smallest performed best. This may be explained physically at the scale of the full icefield by any increase in precipitation with elevation being largely canceled out by decreasing precipitation with distance from the coast. This is consistent with findings in *Roth et al.* [2018] who, on examining a cross-sectional path across the icefield along the dominant wind direction, found that precipitation increases strongly over the first ~15 km of the transect in tandem with steep topographical gains, followed by a gradual decrease over the remaining ~85 km. As SnowModel only applies a single lapse rate over the entire domain, we effectively combine these two effects into a small value. This pattern in precipitation lapse rates may be equally important in other coastal regions with extreme topography rising steeply from sea level and lying along a strong coastal-to-continental gradient. We also find that normal to shallow temperature lapse rates perform the best overall, in agreement with well-established findings that glaciers can impose a dampening effect on local atmospheric lapse rates [*Gardner et al.*, 2009].

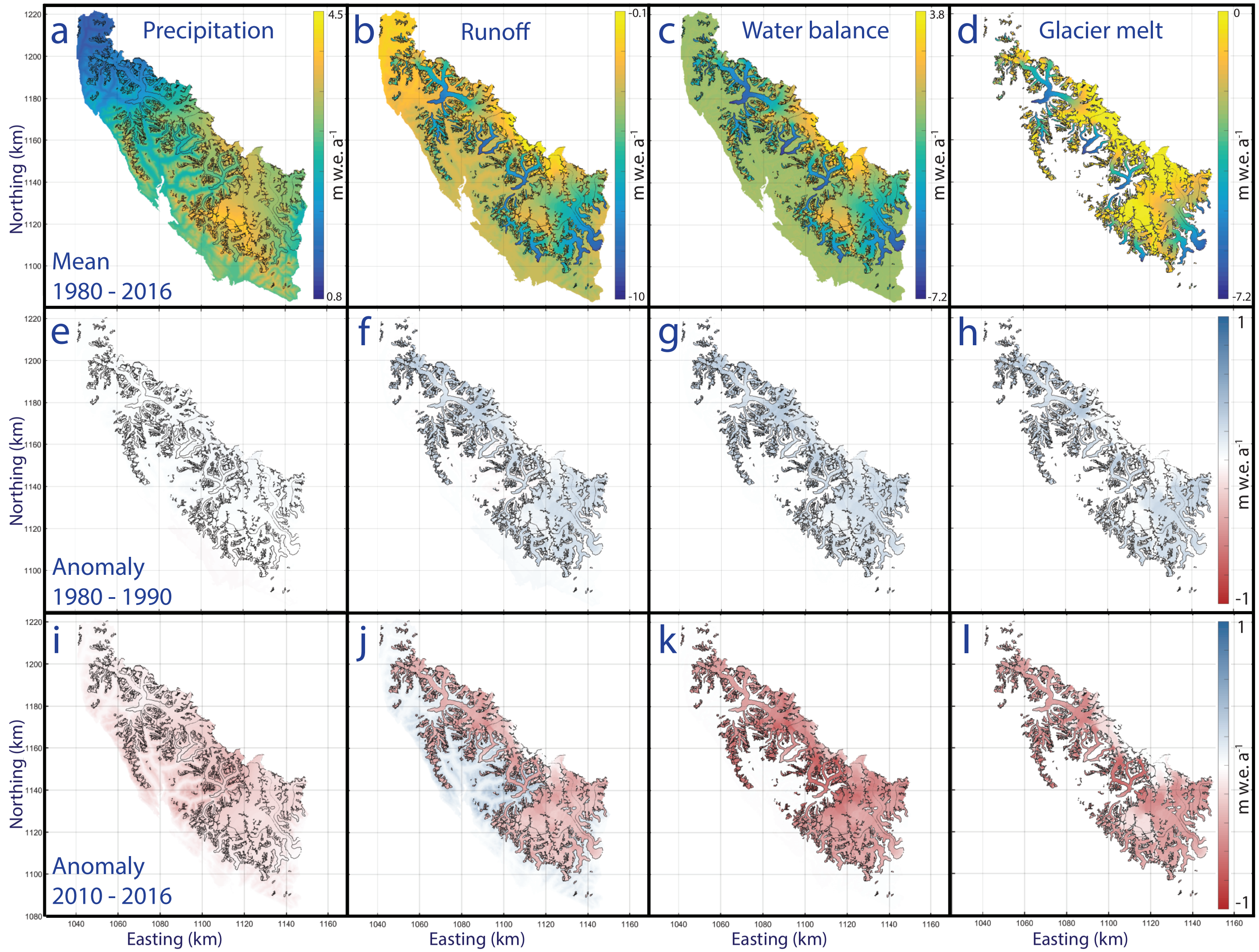

Figure 11. Spatially distributed plots of mean annual rates of precipitation (first column; a, e, and i), total runoff (second column; b, f, and j), water balance (third column; c, g, and k), and glacier ice melt (fourth column; d, h, and l). Figures a-d (first row) display 1980 to 2016 means; note that the scale bars are different for each quantity. Figures e-h (second row) show mean annual anomalies from the 1980 to 2016 mean for the decade 1980 to 1990, while Figures i-l (third row) show anomalies for 2010 to 2016. Figures e-l are displayed using the same color scale. Note that total runoff and glacier ice melt are displayed such that red shading indicates a greater (i.e. more negative) volume than the 1980 to 2016 mean.

Our hydrological simulations reveal that model discharge results are relatively insensitive to the slow reservoir velocity parameter, indicating that most runoff is routed through creeks and streams or over fast-flow terrain such as glacier ice and bare rock. This is supported by the shallow soil reference depth cited in the Harmonized World Soil Dataset [*Fischer et al.*, 2008], and by the modest fraction of forest coverage within the model domain (17% forest, 14% shrubland/grasses/meadows).

6.1.2 Challenges with reproducing stream gauge records

While our model adequately reproduces gauge observations in the two basins with high percent glacier cover ($\geq$ 45%), gauge-matching results in the two lesser glacierized basins ($\leq$ 15%) are weaker. This mismatch is evident as an overproduction of discharge in spring, an underproduction in summer, and an underproduction in winter (see Figure 4). These patterns are similar in the more glacierized basins, but to a lesser extent. Spring and summer discharge discrepancies may be explained by our finding that MicroMet-interpolated MERRA-2 air temperature fields are generally higher in spring and lower in summer compared to observations, and may therefore generate too much early snowmelt in spring, and too little glacier ice melt in summer. We note that this is consistent with a comparative study of reanalysis products for hydrological applications by *Wrzesien et al.* [2019]. These authors find that in North America, MERRA-2 does not maintain snow in mountainous terrain for long enough into spring, which they hypothesized may be due to precipitation biases and warm temperatures. We speculate that these effects may appear stronger in the less glacierized basins given the dominance of snowmelt in spring, with little glacier ice melt contribution in spring or summer.

During winter months, modeled discharge in the less-glacierized basins is near-zero, in contrast to observations that show sporadic discharge. However, modeled precipitation volumes in fall and early winter exceed station observations. A possible explanation for the winter month discharge discrepancy is that because our modeled temperatures are lower than observed during winter months, precipitation events arrive as snow instead of rain, thus adding to the snowpack rather than to discharge. Interestingly, this finding is in contrast to *Wrzesien et al.* [2019], who found that MERRA-2 underestimates mountainous snow. However, their spatial domain encompassed large continental watersheds rather than maritime climates. As few other hydrological studies to date have utilized the MERRA-2 product, we hope our findings may increase understanding of its limitations and utility in maritime climates. We note that MERRA-2 relies partly on assimilated station data and partly on model physics to produce precipitation fields for latitudes up to 62.5° [*Bosilovich et al.*, 2015], and that station data are scarce in this region, particularly at elevation. We underscore the critical need for continuous high-elevation stations in the mountainous regions of Alaska for improving both climatological and hydrological models.

In addition to potential MERRA-2 issues, there are also limitations to downscaling coarse-scale meteorological forcing over complex mountain terrain. For example, the MicroMet module does not account for orographic effects (i.e. decreased precipitation on leeward slopes), relying instead on a simple elevation-dependent precipitation adjustment factor. Altogether, there is much room for improvement in the characterization of precipitation and particularly snow in complex mountain terrain with sparse observation networks. In the meantime, our model's limited ability to reproduce discharge in less-glacierized basins may lead to increased uncertainty in the magnitudes of spring and winter runoff in those basins in particular. Given our principal goal of examining changes for a 44% glacier covered domain, with an emphasis on glacier changes, we accept this cost.

6.1.3 Agreement with GRACE highlights reproduction of large-scale climate processes

The robust agreement between the model and GRACE (Figure 7), in terms of both long-term trends and time series correlation, emphasizes the model's ability to reproduce meso- and synoptic scale climatic processes driving sub- and interannual water balance changes over glacierized terrain. We note that the mass balance rate we derive for the larger GRACE domain (-0.51 [-0.18, +0.13] m w.e. a^{-1}) is less negative than that for only the Juneau Icefield for the same time period (-0.71 m w.e. a^{-1}). We attribute this to inclusion in the GRACE domain of many smaller, higher-elevation glaciers with less negative mass balance rates even at their termini (~-2 m w.e. a^{-1}) relative to the large, low-elevation valley glaciers that dominate the icefield (~-8 m w.e. a^{-1}).

Our finding that modeled seasonal amplitudes for the full land+ice domain are a closer match to those from GRACE than those from the ice-only terrain is consistent with findings for the Gulf of Alaska in *Beamer et al.* [2016] and the Canadian Arctic Archipelago in *Lenaerts et al.* [2013]. In both studies, seasonal amplitudes from GRACE solutions could only be reproduced by summing together model-generated mass changes over both glacierized and ice-free regions of their modeling domains. In earlier generations of GRACE products, GFSC attempted to isolate from the GRACE solution not the full terrestrial water balance but rather the glacier mass change signal alone, with non-ice terrestrial water storage (TWS) changes removed. However, those land-based variations were sourced from a coarse resolution product from the Global Land Data Assimilation System (GLDAS)/Noah dataset of land surface states and fluxes, available at 0.25 x 0.25° [*Rodell et al.*, 2004], and in which variations are set to zero over glaciers. This coarse spatial resolution means that TWS variations from GLDAS/Noah for heavily glacierized regions like the Gulf of Alaska are minimal, and that earlier GRACE solutions for the region therefore inherently contained both glacier and TWS signals. Our simulations confirm this, given that the seasonal amplitudes of the GRACE solution are only achieved by summing together water mass changes over both glacierized and ice-free areas (Figure 7). This result emphasizes the potential for regional scale hydrological modeling to inform our understanding of GRACE.

In terms of long-term trends for the full water balance, our model results show a less negative trend than is estimated using GRACE. This discrepancy is also evident in results using MERRA-1 in *Beamer et al.* [2016], who applied SnowModel at coarser (1 km) resolution over the full Gulf of Alaska region. However, using their best-performing climate product (Climate Forecast System Reanalysis), those authors found favorable agreement between trends. This is a result they believe shows that what has to date been interpreted within GRACE as the long-term ice loss trend is correctly attributed (i.e. that none or little of the trend is attributable to TWS). This interpretation is also consistent with a study by *Reager et al.* [2016], which used reconciled glacier mass balance estimates to isolate global TWS changes from GRACE, and found little in the way of a TWS trend along the Gulf of Alaska. These two regional studies suggest that the increasing trend we see over ice-free land in our model results is likely incorrect, particularly because the model does not account for real storage-enhancing processes (e.g. aquifer recharge, uptake into vegetation in newly deglaciated terrain) that would counteract the expected decreasing water balance from glacier ice loss. One possible explanation for the increase may be due to biases within our MicroMet-interpolated MERRA-2 input data, which may produce more precipitation over cells in our domain that is not contributing to runoff. In particular, the model is likely generating excess, perennial snow over high elevation land cells that are not part of the glacier, when in reality these cells should not have remaining snow by the end of the melt season. This then results in a positive water balance over those areas. This overproduction of snow can be linked to both a) the overall positive (i.e. too large) precipitation biases, and b) the cold biases we observe in air temperature fields versus those at the nearest NOAA weather stations in Juneau and Skagway (see Section 3.2.2.

This finding highlights the challenge of reproducing precipitation in mountain topography, particularly in high latitude ocean-modulated areas where air temperatures are often near the rain-snow threshold, and snow can occur at all months at elevation, conditions that set up great sensitivity within the system due to an ever-changing snowline elevation. Future glacio-hydrological modeling work in coastal areas may benefit from incorporating snowline datasets into their calibration processes.

6.1.4 Model limitations

There are several sources of uncertainty within our model results. The SnowModel-HydroFlow routine focuses largely on internal processes within the snowpack, but neglects several elements that may be important to glacier mass balance. In terms of processes that may contribute to additional ice melt, these include geothermal fluxes at the glacier ice/bed interface, as well as dynamical processes such as frictional melting from viscous heating (internal deformation of the ice) or sliding at the glacier bed [*Mernild et al.*, 2014]. Including these processes would require incorporating geothermal flux and ice dynamics components into the model, which is beyond the scope of this study on surface processes.

SnowModel also does not account for changes in glacier geometry resulting from climate forcing, either in terms of reduced area with glacier retreat, or lowered surface elevations with ice thinning. Rather, our simulations use a reference glacier surface representing conditions in the early 2010s, during which the highest-quality imagery was collected and incorporated into the National Elevation Dataset (our DEM), and used to delineate the most accurate glacier outlines to date [*Pfeffer et al.*, 2014]. However, as this time period lies towards the end of our model period, it is likely that our icefield geometry is too low in elevation and too small in extent for the initial years of our simulation. The former would likely cause an overproduction of glacier ice melt and runoff due to higher temperatures at lower elevations, while the latter would cause an underproduction due to insufficient glacial extent. Quantifying each of these would require accurate DEMs for our full model domain from the 1980s, which unfortunately do not exist. The use of a fixed glacier surface may therefore contribute to uncertainties in our cumulative long-term balance for the full model period, particularly during the initial years of our simulation.

From an energy balance standpoint, SnowModel also does not allow for the inclusion of debris cover, i.e. rocks and dust on glacier ice that can impact melt rates. Thin debris layers can enhance melting by lowering the albedo, while thicker debris layers can reduce melting by insulation [*Østrem*, 1959]. However, we do not have any information on debris thickness throughout our coastal domain, and we note that the amount of debris cover accounts for only 4% of the total ice area (and is even smaller at 2.9% for the full Juneau Icefield) [*Kienholz et al.*, 2015], so we consider the effect small. Finally, additional errors may result given that MicroMet does not react to conditions at the surface that may differ from what the MERRA-2 reanalysis initially prescribes. That is, climate conditions are assigned at each grid cell and time step whether or not snow or ice properties have changed [*Mernild et al.*, 2014], although the presence and condition of snow and ice surfaces has the ability to modify local climatic conditions [e.g. *Oerlemans*, 2010].

6.2 Glacier mass balance

6.2.1 Glacier change present and future

Our model estimates a glacier-wide mass balance rate for 1980 to 2016 of -0.81 [-0.08, +0.11] m w.e. a^{-1} for all ice contained within the domain draining to the coast. To put this estimate in a longer-term context, we compare to future projections from a dynamical (ice flow) study for the Juneau Icefield by *Ziemen et al.* [2016] that modeled possible future mass loss scenarios. In their study, the authors initialized their simulations with a calibrated spin-up for the period 1971 to 2010, followed by projections to 2100. Their model was forced with input climate data downscaled to 20 km from the Coupled Model Intercomparison Project Phase 5 (CMIP5) simulations by the Community Climate System Model 4 [*Gent et al.*, 2011] for 1971 to 2005, and projections to 2100 were forced with the greenhouse gas emissions scenario Representative Concentration Pathway (RCP) 6.0, representing a middle-of-the-road scenario. For the period 1980 to 2016, we find our mass balance rate estimate of -0.81 [-0.08, +0.11] m w.e. a^{-1} to be more negative than the value from *Ziemen et al.* [2016], at -0.46 m w.e. a^{-1}. While their spin-up estimate was generally tuned to fall between reported values from *Melkonian et al.* [2014] to *Larsen et al.* [2007] rather than being something the model independently discovers, we can nonetheless leverage their results in order to gain understanding of potential future changes beyond our period of study. In their projections, they estimated mass balance rates of -1.59 m w.e. a^{-1} for 2016 to 2050 and -2.53 m w.e. a^{-1} from 2050 to 2099, pointing to a more than five-fold mass loss rate increase over their period of study. The only possibility of stabilization they found was in a constant-climate scenario that maintained the climate at 1971 to 2010 levels, wherein the icefield stabilized at 86% of its 2010 volume.

Literature on current and future climate variables pertaining to glacier mass balance, however, suggests that such a constant-climate scenario is highly unlikely. Several studies on Alaska glaciers have for example linked increasing glacier mass loss rates primarily to increases in summer air temperatures [*Arendt et al.*, 2009; *Criscitiello et al.*, 2010; *O'Neel et al.*, 2014; *Young et al.*, 2018], and indeed summer air temperatures are expected to increase as much as 5°C over northern high latitudes by 2100 [*Koenigk et al.*, 2013]. Maritime glaciers in particular are also highly sensitive to precipitation variations, and especially to decreasing amounts of snow serving to deflect solar radiation (e.g. *De Woul and Hock* [2005]). A recent SnowModel study on snow precipitation trends throughout the Arctic region from 1979 to 2009 found evidence of decreasing trends of annual snow precipitation volumes as well as peak snow water equivalent, with trends along the southeast coast generally among the most negative in Alaska [*Liston and Hiemstra*, 2011]. This trend appears to extend into the future given a climate modeling study for the northern coastal temperate rainforest that projects to 2100 a decrease in snow, despite an increase in total precipitation [*Shanley et al.*, 2015]. Analysis of a downscaled gridded climate product has also found that Alaska is experiencing shifts in the rain-snow fraction towards rain [*McAfee et al.*, 2014], a phenomenon to which coastal glaciers have been found to be especially sensitive [*Moore et al.*, 2009], and which can exert a strong influence in our domain given the steep topography and resulting sensitivity to changing snowline elevation. Furthermore, a modeling investigation on maritime Arctic glaciers shows that a 1°C increase in air temperature can only be offset by a 50% increase in snow [*De Woul and Hock*, 2005], an unlikely occurrence given all the mounting evidence for decreased snow and increased rain.

Taken together, we see little evidence that a constant-climate scenario will occur in this region, given current and future trends in increasing air temperature and decreasing snow. As such, there is little indication that glacier mass loss acceleration in the western Juneau Icefield area will decrease or reverse. In fact, our 1980 to 2016 mass loss rate, being more negative than *Ziemen et al.* [2016] to begin with, may point to even stronger accelerations to 2100 than their anticipated five-fold mass loss rate increase. This could result in an even greater reduction in size than their estimated 63% volume loss and 62% area loss by 2100, an outcome that would substantially alter downstream hydrology.

6.2.2 Glaciological linkage to total runoff

We find that mean annual total runoff from our coastal watershed domain is 20.0 km^3 a^{-1} for 1980 to 2016. On a seasonal basis, total runoff ranges from a minimum of 0.004 km^3 in February to a maximum of 5.0 km^3 in July (Figure 6). We observe a single peak in runoff in summer associated with glacier contributions and no secondary peak associated with spring snowmelt. This is consistent with *Hill et al.* [2015] who observed in a modeling study of 1960 to 2010 freshwater discharge a single peak in the hydrograph of the southern Gulf of Alaska region versus a dual peak in the north. Of the total runoff, 55% is sourced from glacier surfaces, a higher value than previous regional estimates for the Gulf of Alaska at 38 to 47% [*Neal et al.*, 2010; *Beamer et al.*, 2016]. The contribution of glacier volume loss to total runoff in our coastal domain is 12% for 1980 to 2016, as compared to regional Gulf of Alaska estimates of 7 to 10% [*Neal et al.*, 2010; *Hill et al.*, 2015; *Beamer et al.*, 2016]. The larger glacier contributions here are likely due to the greater extent of ice cover in our domain (44%) relative to the larger Gulf of Alaska domain (~17%).

Our results indicate that total annual runoff over the 36 year period of study is not correlated with annual glacier mass balance values. This shows that, in coastal environments, even large glaciers or icefields experiencing mass loss may not exert a strong control on total runoff given an overwhelming precipitation signal. This emphasizes the importance of not using annual mass balance values as a proxy for streamflow, and is supported by similar findings for another maritime Alaska glacier basin in *O'Neel et al.* [2014].

We also find that glacier runoff volumes are more strongly correlated with total runoff (r^2 = 0.90) than with glacier ice melt (r^2 = 0.68), suggesting that glacier runoff is more strongly controlled by overall precipitation events than glacier ice melt. This decoupling between glacier ice melt and runoff is likely to be further enhanced in the future, given the projected change in rain/snow fraction towards rain [*McAfee et al.*, 2014; *Shanley et al.*, 2015], which is likely to contribute proportionally more to glacier runoff than to glacier ice melt.

6.3 Freshwater runoff

6.3.1 Glacier ice melt and glacier runoff trends present and future

Examining the annual volume of glacier ice melt over our study period, our results suggest a strongly increasing trend of nearly 10% per decade. Further evidence of increasing glacier ice melt rates is seen in the increasing amplitudes in Figure 10f in recent decades, as well as in the increasing anomalies towards the end of the study period in Figure 11. This finding indicates that in this high latitude maritime glacierized domain, the annual volume of glacier ice melt has not yet reached its maximum and will continue to increase to a yet unknown peak before it begins to decrease. This increasing signal is more difficult to detect (both in terms of magnitude as well as statistical metrics) in annual volumes of glacier runoff (+3% increase) and in total runoff (+1.4% increase). We expect this given increasing contributions from precipitation, which is prone to high variability in this area, as seen in Figure 10 and found in *Bieniek et al.* [2014]. Nonetheless our findings of an increase in total runoff are consistent with an analysis of stream gauge records from the Wolverine Glacier, another maritime glacier watershed in Alaska that experienced a 23% increase in summer streamflow (i.e. a measure of total runoff) between 1966 to 2011 [*O'Neel et al.*, 2014]. While that study was based on gauge measurements and therefore lacked the ability to partition hydrological components, our modeling approach allows us to identify that glacier ice melt is most responsible for the increase in total runoff in our coastal glacierized domain.

As well as contributing new information on current freshwater discharge changes at the local scale in Alaska, our results can be placed in context with other local and regional studies that project future changes as well. First, our finding that glacier ice melt is the principal driver of the total runoff increase is supported by modeling results to 2100 from *Valentin et al.* [2018] for the nearby Copper River watershed in Southcentral Alaska. Those authors projected under the moderate and high emissions scenarios RCP4.5 and RCP8.5 an increase in total runoff of 17 to 48%, respectively, driven primarily by a glacier ice melt increase of 13 to 53%. While that study did not examine the timing of peak water in the watershed, a different study that modeled global glacier runoff changes to 2100 under RCP4.5 found that the Gulf of Alaska is the region projected to reach peak water the latest (between 2060 to 2070) of all regions globally [*Huss and Hock*, 2018]. Although the authors used a calibration approach that leveraged regional rather than local observations of mass balance and did not include comparison to local stream gauge data, their results nonetheless represent a moderate scenario for the region as a whole.

Altogether, our findings and these studies, along with projections for strong and continued warming at high latitudes [*Koenigk et al.*, 2013], lead us to expect that glacier runoff in the western Juneau Icefield will continue to increase before such time as the glaciers lose enough volume to reverse this trend. Although accurately predicting when this will occur would require coupling a hydrological routing model to glacier mass balance modeling projections such as those in *Ziemen et al.* [2016], which is beyond the scope of this hindcasting study, we speculate that given regional projections for the Gulf of Alaska of a peak water period near 2060 to 2070 [*Huss and Hock*, 2018], it will be several decades before the phenomenon occurs in our domain.

6.3.2 A changing hydrological regime

Even with a strong increasing trend in annual glacier ice melt volumes, total runoff in this coastal glacierized area shows evidence of only a slightly increasing trend. Our findings instead reveal that the most prominent signs of hydrological regime change in this region are with respect to the timing and biogeochemical characteristics of the water being delivered downstream.

One indicator of these water quality changes is an increase in the magnitude of the maximum daily volume of glacier ice melt at a rate of 10% per decade. This increase has the potential, on those maximum flow days, to substantially modify freshwater conditions downstream as the proportion of glacier ice melt input grows relative to other freshwater sources. Additionally, although we do not detect robust trends in the onset, end, or subsequent length of the glacier ice melt season, our results suggest a marked increase in glacier ice melt delivery during the spring months, which in essence serves to shift periods of high glacier ice melt earlier into the year (Table 3, Figure 10). This earlier arrival signals a shift towards a hydrograph more closely resembling that of snowmelt-dominated basins. This finding is supported by regional analyses of temperature records in western North America over the past 50 years that show an asymmetry in warming of spring versus fall, which can be explained by seasonal differences in atmospheric circulation regimes [*Abatzoglou and Redmond*, 2007]. However, in projections to 2100, *Koenigk et al.* [2013] found the most pronounced increases in air temperature in Alaska are likely to occur in winter and fall. We suggest, therefore, that there is potential for future increases in glacier ice melt and glacier runoff volumes in the fall season as well.

Several downstream impacts have occurred since the 1980s with a 16% increase per decade in springtime glacier ice melt and a corresponding 7% increase in glacier runoff. Given the tight relationship between stream temperature and glacier cover in this area [*Fellman et al.*, 2014], our results suggest that stream temperatures during the spring months have likely become lower on account of the higher proportion of glacier ice melt input. In addition, we speculate there has been an increase in turbidity stemming from the influx of glacially-eroded sediment along with increased glacier melt [*Milner et al.*, 2017]. Minerals and limiting nutrients contained therein are in turn likely delivered earlier and at larger magnitudes, including phosphorous, nitrogen, iron, and bioavailable organic carbon to riverine and estuarine food webs [*O'Neel et al.*, 2015].

In addition to altering stream conditions, the biogeophysical signature of glacier runoff also extends kilometers into Gulf of Alaska fjords, by setting up a stratified water column with fresh, cold, turbid, and generally nutrient-rich water at the ocean surface

[*Arimitsu et al.*, 2016]. Therefore, changes in the timing of arrival of large volumes of glacier runoff will influence both estuary and stream conditions. In the estuary, glacially-influenced environmental gradients explain much of the distribution and abundance of phytoplankton, which in turn drives higher trophic level food web structure for copepods, fish, and sea birds [*Arimitsu et al.*, 2016]. In rivers and streams, both temperature and water clarity are key variables for Pacific salmon spawning ground habitat selection [*Lorenz and Filer*, 1989], particularly given the sharp thermal limits of these species [*Welch et al.*, 1998; *Richter and Kolmes*, 2005]. Indeed, evidence is already mounting that populations among several Pacific salmon species are migrating to freshwater up to 0.5 days earlier per year than they did historically [*Kovach et al.*, 2015]. Although the mechanisms for the earlier timing remain complex, freshwater conditions in the riverine environment may contribute, given freshwater conditions that may support migration earlier in the year. For other populations, however, there is some concern that eventual decreased summer flows may lead to higher water temperatures and in turn lead to reduced salmonid function [*Richter and Kolmes*, 2005] as well as a reduction in spawning habitat [*Wobus et al.*, 2015]. These latter concerns may come to pass after the period of peak water has passed in this domain.

Given our findings that peak glacier ice melt volumes are arriving earlier and that annual and spring volumes of freshwater (glacier ice melt, glacier runoff, and total runoff) are increasing, changes to freshwater thermal regimes and riverine nutrient export have likely already taken place in this high latitude coastal ecosystem. Moreover, under continued warming and a decrease in precipitation as snow, projections continue to call for substantial and varied change to these and other hydroecological variables into the future [*Shanley et al.*, 2015].

7 Conclusions

This study applied the coupled glacio-hydrological model SnowModel-HydroFlow to estimate daily freshwater runoff from 1980 to 2016 for the coastal watershed draining the western Juneau Icefield in Southeast Alaska, an area of 6405 km^2 with 44% glacier cover. We find a strongly increasing trend in annual glacier ice melt production (9.6% per decade), with especially pronounced increases during spring months (16.5% per decade). This increase can also be detected in both glacier runoff (3.0% for annual volumes, 6.8% for spring volumes) and total runoff (1.4%, 2.7%). Together, these results suggest that this particular region has not yet passed the period of peak water associated with a persistent negative mass balance, likely on account of the extensive glacier coverage.

Unlike studies based on stream gauge data, our model results afford the opportunity to identify that glacier ice melt is the likely hydrological driver behind increases in total runoff seen over the past several decades. Moreover, our study contributes new and affirmative knowledge towards the question of whether glacier runoff trends can be detected in maritime climates with high precipitation variability.

Overall in this domain, glacier runoff contributes 55% of total runoff, including 12% from non-renewable glacier volume loss. Total runoff in the domain is found not to be correlated to annual glacier mass balance, supporting the paradigm that advises against using annual balances as a proxy for glacier runoff volumes. Given projection studies that predict increasing glacier volume loss for the Juneau Icefield through 2100, we anticipate ongoing glacier ice melt increases decades into the future, until such point as peak water is passed and the contribution of glacier ice melt and glacier runoff to the domain begins to change once more.

We find that changes in runoff timing and biogeochemical properties are the aspects of the hydrological regime undergoing the greatest changes in this coastal glacierized environment, with substantial impacts for downstream ecosystems. In particular, the earlier arrival of large volumes of glacier ice melt in spring is likely exerting an influence on stream temperature and clarity, a point of concern for downstream species such as salmon that have evolved to survive in particular freshwater conditions.

Ultimately, our results emphasize that even in maritime climates with high precipitation variability, high latitude glacierized watersheds are experiencing perceptible and ongoing hydrological regime change given persistent glacier volume loss.

Acknowledgments

The authors would like to thank W.P. Dryer, C. McNeil, S. Candela, and J. Pierce for help in the field. R. Crumley and C. Cosgrove assisted with SnowModel initialization. The Juneau Icefield Research Program (JIRP) provided field data and logistical support. E. Berthier provided geodetic data, F. Ziemen contributed model results, and C. McNeil provided datasets on behalf of both USGS and JIRP. This work was supported by a Department of Interior Alaska Climate Adaptation Science Center graduate fellowship awarded under Cooperative Agreement G17AC00213, by NASA under award NASANNX16AQ88G, by the National Science Foundation under award OIA-1208927 and by the State of Alaska (Experimental Program for Stimulating Competitive Research – Alaska Adapting to Changing Environments award), and by the University of Alaska Fairbanks Resilience and Adaptation Program.

All previously published data used in this study are available from the sources mentioned within the Data section of this article. Model code for SnowModel-HydroFlow can be found at ftp://ftp.cira.colostate.edu/ftp/Liston/JCYoung_WRR_2020/model_code/, and for the SoilBal module at https://doi.org/10.4211/hs.8e12debf926c4299acc782f9407512f5.

References

Abatzoglou, J., and K. Redmond (2007), Asymmetry between trends in spring and autumn temperature and circulation regimes over western North America, *Geophysical Research Letters*, *34*(18).

Amrhein, V., S. Greenland, and B. McShane (2019), Retire statistical significance, *Nature*, *567*.

Arendt, A., J. Walsh, and W. Harrison (2009), Changes of Glaciers and Climate in Northwestern North America during the Late 20th Century, *Journal of Climate*, *22*(15), 4117–4134.

Arendt, A., S. Luthcke, A. Gardner, S. O'Neel, D. Hill, G. Moholdt, and W. Abdalati (2013), Analysis of a GRACE global mascon solution for gulf of alaska glaciers, *Journal of Glaciology*, *59*(217), 913.

Arimitsu, M. L., J. F. Piatt, and F. Mueter (2016), Influence of glacier runoff on ecosystem structure in Gulf of Alaska fjords, *Marine Ecology Progress Series*, *560*, 19–40.

Beamer, J., D. Hill, A. Arendt, and G. Liston (2016), High-resolution modeling of coastal freshwater discharge and glacier mass balance in the Gulf of Alaska watershed, *Water Resources Research*.

Berthier, E., E. Schiefer, G. Clarke, B. Menounos, and F. Rémy (2010), Contribution of Alaskan glaciers to sea level rise derived from satellite imagery, *Nature Geoscience*, *3*, 92–95, doi:10.1038/NGEO737.

Berthier, E., C. Larsen, W. J. Durkin, M. J. Willis, and M. E. Pritchard (2018), Brief communication: Unabated wastage of the Juneau and Stikine icefields (southeast Alaska) in the early 21st century, *The Cryosphere*, *12*(4), 1523–1530.

Bieniek, P. A., J. E. Walsh, R. L. Thoman, and U. S. Bhatt (2014), Using climate divisions to analyze variations and trends in alaska temperature and precipitation, *Journal of Climate*, *27*(8), 2800–2818.

Bosilovich, M., R. Lucchesi, and M. Suarez (2015), MERRA-2: File specification.

Boyce, E. S., R. J. Motyka, and M. Truffer (2007), Flotation and retreat of a lake-calving terminus, Mendenhall Glacier, southeast Alaska, USA, *Journal of Glaciology*, *53*(181), 211–224.

Carnahan, E., J. Amundson, and E. Hood (2018), Impact of glacier loss on annual basin water yields, *Hydrology and Earth System Sciences Discussions*, pp. 1–20, doi: 10.5194/hess-2018-509.

Cohen, J. (2016), The earth is round (p ≤ .05), in *What if there were no significance tests?*, pp. 69–82, Routledge.

Criscitiello, A. S., M. A. Kelly, and B. Tremblay (2010), The response of Taku and Lemon Creek glaciers to climate, *Arctic, Antarctic, and Alpine Research*, *42*(1), 34–44.

Crusius, J., A. W. Schroth, S. Gasso, C. M. Moy, R. C. Levy, and M. Gatica (2011), Glacial flour dust storms in the Gulf of Alaska: Hydrologic and meteorological controls and their importance as a source of bioavailable iron, *Geophysical Research Letters*, *38*(6).

Cuffey, K. M., and W. S. B. Paterson (2010), *The Physics of Glaciers*, Academic Press.

Daly, C., M. Halbleib, J. I. Smith, W. P. Gibson, M. K. Doggett, G. H. Taylor, J. Curtis, and P. P. Pasteris (2008), Physiographically sensitive mapping of climatological temperature and precipitation across the conterminous united states, *International Journal of Climatology: A Journal of the Royal Meteorological Society*, *28*(15), 2031–2064.

De Woul, M., and R. Hock (2005), Static mass-balance sensitivity of arctic glaciers and ice caps using a degree-day approach, *Annals of Glaciology*, *42*(1), 217–224.

Fellman, J. B., S. Nagorski, S. Pyare, A. W. Vermilyea, D. Scott, and E. Hood (2014), Stream temperature response to variable glacier coverage in coastal watersheds of Southeast Alaska, *Hydrological Processes*, *28*(4), 2062–2073.

Fellman, J. B., E. Hood, P. A. Raymond, J. Hudson, M. Bozeman, and M. Arimitsu (2015), Evidence for the assimilation of ancient glacier organic carbon in a proglacial stream food web, *Limnology and Oceanography*, *60*(4), 1118–1128.

Fischer, G., S. Nachtergaele, H. Prieler, L. van Velthuizen, and D. Verelst (2008), Global Agro-Ecological Zones assessment for agriculture (GAEZ 2008), *IIASA, Laxenburg, Austria and FAO, Rome, Italy*.

Fountain, A. G., and W. V. Tangborn (1985), The effect of glaciers on streamflow variations, *Water Resources Research*, *21*(4), 579–586.

Ganey, G. Q., M. G. Loso, A. B. Burgess, and R. J. Dial (2017), The role of microbes in snowmelt and radiative forcing on an Alaskan icefield, *Nature Geoscience*, *10*(10), 754.

Gardner, A. S., M. J. Sharp, R. M. Koerner, C. Labine, S. Boon, S. J. Marshall, D. O. Burgess, and D. Lewis (2009), Near-surface temperature lapse rates over arctic glaciers and their implications for temperature downscaling, *Journal of Climate*, *22*(16), 4281?4298.

Gelaro, R., W. McCarty, M. J. Suárez, R. Todling, A. Molod, L. Takacs, C. A. Randles, A. Darmenov, M. G. Bosilovich, R. Reichle, et al. (2017), The modern-era retrospective analysis for research and applications, version 2 (MERRA-2), *Journal of Climate*, *30*(14), 5419–5454.

Gent, P. R., G. Danabasoglu, L. J. Donner, M. M. Holland, E. C. Hunke, S. R. Jayne, D. M. Lawrence, R. B. Neale, P. J. Rasch, M. Vertenstein, et al. (2011), The community climate system model version 4, *Journal of Climate*, *24*(19), 4973–4991.

Gleick, P. H., and M. Palaniappan (2010), Peak water limits to freshwater withdrawal and use, *Proceedings of the National Academy of Sciences*, *107*(25), 11,155–11,162.

Halsey, L. G. (2019), The reign of the p-value is over: What alternative analyses could we employ to fill the power vacuum?, *Biology Letters*, *15*(5), 20190,174.

Halsey, L. G., D. Curran-Everett, S. L. Vowler, and G. B. Drummond (2015), The fickle p value generates irreproducible results, *Nature Methods*, *12*(3), 179.

Helsel, D. R., and R. M. Hirsch (2002), *Statistical methods in water resources*, vol. 323, US Geological Survey Reston, VA.

Hill, D., N. Bruhis, S. Calos, A. Arendt, and J. Beamer (2015), Spatial and temporal variability of freshwater discharge into the Gulf of Alaska, *Journal of Geophysical Research: Oceans*, *120*(2), 634–646.

Hock, R., and M. Huss (2015), A new model for global glacier change and sea-level rise, *Frontiers in Earth Science*, *3*, 1–22.

Homer, C., J. Dewitz, L. Yang, S. Jin, P. Danielson, G. Xian, J. Coulston, N. Herold, J. Wickham, and K. Megown (2015), Completion of the 2011 National Land Cover Database for the conterminous United States–representing a decade of land cover change information, *Photogrammetric Engineering & Remote Sensing*, *81*(5), 345–354.

Hood, E., and L. Berner (2009), The effect of changing glacial coverage on the physical and biogeochemical properties of coastal streams in southeastern Alaska, *Journal of Geophysical Research*, *114*(13), G03,001, doi:10.1029/2009JG000971.

Hood, E., and D. Scott (2008), Riverine organic matter and nutrients in Southeast Alaska affected by glacial coverage, *Nature Geoscience*, *1*(9), 583–587.

Hood, E., J. Fellman, R. Spencer, P. Hernes, R. Edwards, D. D'Amore, and D. Scott (2009), Glaciers as a source of ancient and labile organic matter to the marine environment, *Nature*, *462*(7276), 1044–1048, doi:10.1038/nature08580.

Hoogeveen, J., J.-M. Faurès, L. Peiser, J. Burke, and N. Giesen (2015), GlobWat–a global water balance model to assess water use in irrigated agriculture, *Hydrology and Earth System Sciences*, *19*(9), 3829–3844.

Huss, M., and R. Hock (2018), Global-scale hydrological response to future glacier mass loss, *Nature Climate Change*, *8*(2), 135.

Jansson, P., R. Hock, and T. Schneider (2003), The concept of glacier storage: A review, *Journal of Hydrology*, *282*(1-4), 116–129.

Kienholz, C., S. Herreid, J. Rich, A. Arendt, R. Hock, and E. Burgess (2015), Derivation and analysis of a complete modern-date glacier inventory for Alaska and northwest Canada, *Journal of Glaciology*, *61*(227), 403.

Koenigk, T., L. Brodeau, R. G. Graversen, J. Karlsson, G. Svensson, M. Tjernström, U. Willén, and K. Wyser (2013), Arctic climate change in 21st century CMIP5 simulations with EC-Earth, *Climate Dynamics*, *40*(11-12), 2719–2743.

Komatsu, H. (2005), Forest categorization according to dry-canopy evaporation rates in the growing season: Comparison of the Priestley–Taylor coefficient values from various observation sites, *Hydrological Processes: An International Journal*, *19*(19), 3873–3896.

Kovach, R. P., S. C. Ellison, S. Pyare, and D. A. Tallmon (2015), Temporal patterns in adult salmon migration timing across southeast alaska, *Global Change Biology*, *21*(5), 1821–1833.

Lader, R., U. S. Bhatt, J. E. Walsh, T. S. Rupp, and P. A. Bieniek (2016), Two-meter temperature and precipitation from atmospheric reanalysis evaluated for Alaska, *Journal of Applied Meteorology and Climatology*, *55*(4), 901–922.

Lang, H. (1986), Forecasting meltwater runoff from snow-covered areas and from glacier basins, in *River flow modelling and forecasting*, pp. 99–127, Springer.

Larsen, C., R. Motyka, J. Freymuller, K. Echelmeyer, and E. Ivins (2005), Rapid viscoelastic uplift in Southeast Alaska caused by post-Little Ice Age glacial retreat, *Earth and Planetary Science Letters*, *237*, 548–560.

Larsen, C., R. Motyka, A. Arendt, K. Echelmeyer, and P. Geissler (2007), Glacier changes in southeast Alaska and northwest British Columbia and contribution to sea level rise, *Journal of Geophysical Research*, *112*(1), F01,007, doi:10.1029/2006JF000586.

Lawson, E. C., J. L. Wadham, M. Tranter, M. Stibal, G. P. Lis, C. E. Butler, J. Laybourn-Parry, P. Nienow, D. Chandler, and P. Dewsbury (2014), Greenland Ice Sheet exports labile organic carbon to the Arctic oceans, *Biogeosciences*, *11*(14), 4015–4028.

Lenaerts, J., J. H. Angelen, M. R. Broeke, A. S. Gardner, B. Wouters, and E. Meijgaard (2013), Irreversible mass loss of Canadian Arctic Archipelago glaciers, *Geophysical Research Letters*, *40*(5), 870–874.

Lindsay, R., M. Wensnahan, A. Schweiger, and J. Zhang (2014), Evaluation of seven different atmospheric reanalysis products in the Arctic, *Journal of Climate*, *27*(7), 2588–2606.

Liston, G. E., and K. Elder (2006a), A distributed snow-evolution modeling system (SnowModel), *Journal of Hydrometeorology*, *7*(6), 1259–1276.

Liston, G. E., and K. Elder (2006b), A meteorological distribution system for high-resolution terrestrial modeling (MicroMet), *Journal of Hydrometeorology*, *7*(2), 217–234.

Liston, G. E., and C. A. Hiemstra (2008), A simple data assimilation system for complex snow distributions (SnowAssim), *Journal of Hydrometeorology*, *9*(5), 989–1004.

Liston, G. E., and C. A. Hiemstra (2011), The changing cryosphere: Pan-Arctic snow trends (1979-2009), *Journal of Climate*, *24*(21), 5691–5712.

Liston, G. E., and S. H. Mernild (2012), Greenland freshwater runoff. Part I: A runoff routing model for glaciated and nonglaciated landscapes (HydroFlow), *Journal of Climate*, *25*(17), 5997–6014.

Liston, G. E., and M. Sturm (2002), Winter precipitation patterns in arctic Alaska determined from a blowing-snow model and snow-depth observations, *Journal of Hydrometeorology*, *3*(6), 646–659.

Loomis, B., S. Luthcke, and T. Sabaka (2019), Regularization and error characterization of GRACE mascons, *Journal of Geodesy*, pp. 1–18.

Lorenz, J. M., and J. H. Filer (1989), Spawning habitat and redd characteristics of sockeye salmon in the glacial Taku River, British Columbia and Alaska, *Transactions of the American Fisheries Society*, *118*(5), 495–502.

Luthcke, S., T. Sabaka, B. Loomis, A. Arendt, J. McCarthy, and J. Camp (2013), Antarctica, Greenland and Gulf of Alaska land-ice evolution from an iterated GRACE global mascon solution, *Journal of Glaciology*, *59*(216), 613–631, doi:10.3189/2013JoG12J147.

Masson-Delmotte, V., P. Zhai, H.-O. PÃűrtner, D. Roberts, J. Skea, P. Shukla, A. Pirani, W. Moufouma-Okia, C. PÃľan, R. Pidcock, S. Connors, J. Matthews, Y. Chen, X. Zhou, M. Gomis, E. Lonnoy, T. Maycock, M. Tignor, and T. Waterfield (2018), IPCC, 2018: Summary for Policymakers. In: Global Warming of 1.5ÂřC. An IPCC Special Report on the impacts of global warming of 1.5ÂřC above pre-industrial levels and related global greenhouse gas emission pathways, in the context of strengthening the global response to the threat of climate change, sustainable development, and efforts to eradicate poverty, *Technical report*, World Meteorological Organization.

McAfee, S. A., J. Walsh, and T. S. Rupp (2014), Statistically downscaled projections of snow/rain partitioning for Alaska, *Hydrological Processes*, *28*(12), 3930–3946.

McGrath, D., L. Sass, S. O'Neel, A. Arendt, G. Wolken, A. Gusmeroli, C. Kienholz, and C. McNeil (2015), End-of-winter snow depth variability on glaciers in Alaska, *Journal of Geophysical Research: Earth Surface*, *120*(8), 1530–1550.

McNeil, C. J., S. W. Campbell, S. O'Neel, and E. H. Baker (2019), Glacier-wide mass balance and compiled data inputs: Juneau icefield glaciers, doi:10.5066/P9YBZ36F.

McNeil, S. L. C. F. C. E. B. E. H. P. E. H. W. E. N. M. Z. S. F. D. B. C. A. M., C. J., and S. R. O'Neel (2019), Glacier-wide mass balance and compiled data inputs: Juneau icefield glaciers (ver. 4.0, november 2019), doi:10.5066/F7HD7SRF.

Melkonian, A. K., M. J. Willis, and M. E. Pritchard (2014), Satellite-derived volume loss rates and glacier speeds for the Juneau Icefield, Alaska, *Journal of Glaciology*, *60*(222), 743–760.

Mernild, S. H., and G. E. Liston (2012), Greenland freshwater runoff. Part II: Distribution and trends, 1960–2010, *Journal of Climate*, *25*(17), 6015–6035.

Mernild, S. H., G. E. Liston, B. Hasholt, and N. T. Knudsen (2006), Snow distribution and melt modeling for Mittivakkat Glacier, Ammassalik Island, southeast Greenland, *Journal of Hydrometeorology*, *7*(4), 808–824.

Mernild, S. H., G. E. Liston, and B. Hasholt (2007), Snow-distribution and melt modelling for glaciers in Zackenberg river drainage basin, north-eastern Greenland, *Hydrological*

Processes, *21*(24), 3249–3263, doi:10.1002/hyp.6500.

Mernild, S. H., G. E. Liston, C. A. Hiemstra, and J. H. Christensen (2010), Greenland ice sheet surface mass-balance modeling in a 131-yr perspective, 1950-2080, *Journal of Hydrometeorology*, *11*(1), 3–25.

Mernild, S. H., G. E. Liston, and C. A. Hiemstra (2014), Northern hemisphere glacier and ice cap surface mass balance and contribution to sea level rise, *Journal of Climate*, *27*(15), 6051–6073.

Mernild, S. H., D. M. Holland, D. Holland, A. Rosing-Asvid, J. C. Yde, G. E. Liston, and K. Steffen (2015), Freshwater flux and spatiotemporal simulated runoff variability into Ilulissat Icefjord, West Greenland, linked to salinity and temperature Observations near tidewater glacier margins obtained using instrumented ringed seals, *Journal of Physical Oceanography*, *45*(5), 1426–1445.

Mernild, S. H., G. E. Liston, C. Hiemstra, and R. Wilson (2017), The andes cordillera. part iii: glacier surface mass balance and contribution to sea level rise (1979–2014), *International Journal of Climatology*, *37*(7), 3154–3174.

Mesinger, F., G. DiMego, E. Kalnay, K. Mitchell, P. C. Shafran, W. Ebisuzaki, D. Jović, J. Woollen, E. Rogers, E. H. Berbery, et al. (2006), North American Regional Reanalysis, *Bulletin of the American Meteorological Society*, *87*(3), 343–360.

Milner, A. M., K. Khamis, T. J. Battin, J. E. Brittain, N. E. Barrand, L. Füreder, S. Cauvy-Fraunié, G. M. Gíslason, D. Jacobsen, D. M. Hannah, et al. (2017), Glacier shrinkage driving global changes in downstream systems, *Proceedings of the National Academy of Sciences*, *114*(37), 9770–9778.

Moore, R. D., S. W. Fleming, B. Menounos, R. Wheate, A. Fountain, K. Stahl, K. Holm, and M. Jakob (2009), Glacier change in western North America: implications for hydrology, geomorphic hazards and water quality, *Hydrological Processes*, *23*, 42–61.

Motyka, R. J., S. O'Neel, C. L. Connor, and K. A. Echelmeyer (2002), Twentieth century thinning of Mendenhall Glacier, Alaska, and its relationship to climate, lake calving, and glacier run-off, *Global and Planetary Change*, *35*(1-2), 93–112.

Nagorski, S. A., S. D. Kaspari, E. Hood, J. B. Fellman, and S. M. Skiles (2019), Radiative Forcing by Dust and Black Carbon on the Juneau Icefield, Alaska, *Journal of Geophysical Research: Atmospheres*, *124*(7), 3943–3959.

Nash, J. E., and J. V. Sutcliffe (1970), River flow forecasting through conceptual models part I: A discussion of principles, *Journal of Hydrology*, *10*(3), 282–290.

Neal, E., E. Hood, and K. Smikrud (2010), Contribution of glacier runoff to freshwater discharge into Gulf of Alaska, *Geophysical Research Letters*, *37*(6), L06,404, doi:10.1029/2010GL042385.

Oerlemans, J. (2010), *The Microclimate of Valley Glaciers*, Igitur, Utrecht Publishing & Archiving Services.

O'Neel, S., E. Hood, A. Arendt, and L. Sass (2014), Assessing streamflow sensitivity to variations in glacier mass balance, *Climatic Change*, *123*(2), 329–341.

O'Neel, S., E. Hood, A. L. Bidlack, S. W. Fleming, M. L. Arimitsu, A. Arendt, E. Burgess, C. J. Sergeant, A. H. Beaudreau, K. Timm, et al. (2015), Icefield-to-ocean linkages across the northern Pacific coastal temperate rainforest ecosystem, *BioScience*, *65*(5), 499–512.

O'Neel, S., D. McGrath, G. Wolken, E. Whorton, S. Candela, L. Sass, C. McNeil, E. Baker, E. Peitzsch, D. Fagre, A. Clark, C. Florentine, Z. Miller, J. Christian, K. Christianson, E. Babcock, M. Loso, A. Arendt, E. Burgess, and A. Gusmeroli (2018), Ground Penetrating Radar Data on North American Glaciers, version 2.1, U.S. Geological Survey data release, doi:10.5066/F7M043G7.

Østrem, G. (1959), Ice melting under a thin layer of moraine, and the existence of ice cores in moraine ridges, *Geografiska Annaler*, *41*(4), 228–230.

Østrem, G., and M. Brugman (1991), Glacier mass-balance measurements, *Technical report*, National Hydrology Research Institute.

Peltier, W. (2004), Global glacial isostasy and the surface of the Ice-Age Earth: the ICE-5G (VM2) model and GRACE, *Annual Review of Earth and Planetary Sciences*, *32*, 111–149.

Pelto, M., J. Kavanaugh, and C. McNeil (2013), Juneau Icefield mass balance program 1946–2011, *Earth System Science Data*, *5*(2), 319–330.

Pfeffer, W. T., A. A. Arendt, A. Bliss, T. Bolch, J. G. Cogley, A. S. Gardner, J.-O. Hagen, R. Hock, G. Kaser, C. Kienholz, et al. (2014), The Randolph Glacier Inventory: A globally complete inventory of glaciers, *Journal of Glaciology*, *60*(221), 537–552.

Priestley, C., R. Taylor, et al. (1972), On the assessment of surface heat flux and evaporation using large-scale parameters, *Monthly Weather Review*, *100*(2), 81–92.

Radić, V., and R. Hock (2014), Glaciers in the Earth's hydrological cycle: Assessments of glacier mass and runoff changes on global and regional scales, *Surveys in Geophysics*, *35*(3), 813–837.

Ramage, J. M., B. L. Isacks, and M. M. Miller (2000), Radar glacier zones in southeast Alaska, USA: Field and satellite observations, *Journal of Glaciology*, *46*(153), 287–296.

Reager, J., A. Gardner, J. Famiglietti, D. Wiese, A. Eicker, and M.-H. Lo (2016), A decade of sea level rise slowed by climate-driven hydrology, *Science*, *351*(6274), 699–703.

Reichle, R. H., C. S. Draper, Q. Liu, M. Girotto, S. P. Mahanama, R. D. Koster, and G. J. De Lannoy (2017), Assessment of MERRA-2 land surface hydrology estimates, *Journal of Climate*, *30*(8), 2937–2960.

Richter, A., and S. A. Kolmes (2005), Maximum temperature limits for Chinook, coho, and chum salmon, and steelhead trout in the Pacific Northwest, *Reviews in Fisheries science*, *13*(1), 23–49.

Rienecker, M. M., M. J. Suarez, R. Gelaro, R. Todling, J. Bacmeister, E. Liu, M. G. Bosilovich, S. D. Schubert, L. Takacs, G.-K. Kim, et al. (2011), MERRA: NASA's Modern-Era Retrospective Analysis for Research and applications, *Journal of Climate*, *24*(14), 3624–3648.

Rodell, M., P. Houser, U. Jambor, J. Gottschalck, K. Mitchell, C.-J. Meng, K. Arsenault, B. Cosgrove, J. Radakovich, M. Bosilovich, J. K. Entin, J. P. Walker, D. Lohmann, and D. Toll (2004), The Global Land Data Assimilation System, *Bulletin of the American Meteorological Society*, *85*(3), 381–394.

Rohrer, M. (1989), Determination of the transition air temperature from snow to rain and intensity of precipitation, in *WMO IASH ETH International Workshop on Precipitation Measurement*, pp. 475–582.

Roth, A., R. Hock, T. V. Schuler, P. A. Bieniek, M. Pelto, and A. Aschwanden (2018), Modeling winter precipitation over the Juneau Icefield, Alaska, using a linear model of orographic precipitation, *Frontiers in Earth Science*, *6*, 20.

Royer, T. C. (1998), Coastal processes in the northern north pacific, *The Global Coastal Ocean: Regional Studies and Synthesis*.

Saha, S., S. Moorthi, H.-L. Pan, X. Wu, J. Wang, S. Nadiga, P. Tripp, R. Kistler, J. Woollen, D. Behringer, et al. (2010), The NCEP climate forecast system reanalysis, *Bulletin of the American Meteorological Society*, *91*(8), 1015–1058.

Shanley, C. S., S. Pyare, M. I. Goldstein, P. B. Alaback, D. M. Albert, C. M. Beier, T. J. Brinkman, R. T. Edwards, E. Hood, A. MacKinnon, et al. (2015), Climate change implications in the northern coastal temperate rainforest of North America, *Climatic Change*, *130*(2), 155–170.

Shi, T., D. Guan, A. Wang, J. Wu, C. Jin, and S. Han (2008), Comparison of three models to estimate evapotranspiration for a temperate mixed forest, *Hydrological Processes: An International Journal*, *22*(17), 3431–3443.

Stabeno, P., N. Bond, A. Hermann, N. Kachel, C. Mordy, and J. Overland (2004), Meteorology and oceanography of the Northern Gulf of Alaska, *Continental Shelf Research*, *24*(7-8), 859–897.

Tomczak, M., and E. Tomczak (2014), The need to report effect size estimates revisited. An overview of some recommended measures of effect size, *Trends in Sport Sciences*, *21*(1).

Truffer, M., R. J. Motyka, M. Hekkers, I. M. Howat, and M. A. King (2009), Terminus dynamics at an advancing glacier: Taku Glacier, Alaska, *Journal of Glaciology*, *55*(194), 1052–1060.

Valentin, M., T. Hogue, and L. Hay (2018), Hydrologic regime changes in a high-latitude glacierized watershed under future climate conditions, *Water*, *10*(2), 128.

Welch, D., Y. Ishida, and K. Nagasawa (1998), Thermal limits and ocean migrations of sockeye salmon (Oncorhynchus nerka): Long-term consequences of global warming, *Canadian Journal of Fisheries and Aquatic Sciences*, *55*(4), 937–948.

Wilson, D. J. (2019), The harmonic mean p-value for combining dependent tests, *Proceedings of the National Academy of Sciences*, *116*(4), 1195–1200.

Wobus, C., R. Prucha, D. Albert, C. Woll, M. Loinaz, and R. Jones (2015), Hydrologic alterations from climate change inform assessment of ecological risk to pacific salmon in Bristol Bay, Alaska, *PloS one*, *10*(12), e0143,905.

Wouters, B., J. Bonin, D. Chambers, R. Riva, I. Sasgen, and J. Wahr (2014), GRACE, time-varying gravity, Earth system dynamics and climate change, *Reports on Progress in Physics*, *77*(11), 116,801.

Wrzesien, M. L., M. T. Durand, and T. M. Pavelsky (2019), A reassessment of North American river basin cool-season precipitation: Developments from a new mountain climatology dataset, *Water Resources Research*, doi:10.1029/2018WR024106.

Young, J. C. (2019), Gilkey Glacier mass balance point observations 2013-2015, Southeast Alaska, HydroShare, doi:10.4211/hs.275f3521cc834467a34c051a716a3b30.

Young, J. C., A. Arendt, R. Hock, and E. Pettit (2018), The challenge of monitoring glaciers with extreme altitudinal range: mass-balance reconstruction for Kahiltna Glacier, Alaska, *Journal of Glaciology*, doi:10.1017/jog.2017.80.

Ziemen, F. A., R. Hock, A. Aschwanden, C. Khroulev, C. Kienholz, A. Melkonian, and J. Zhang (2016), Modeling the evolution of the Juneau Icefield between 1971 and 2100 using the Parallel Ice Sheet Model (PISM), *Journal of Glaciology*, *62*(231), 199–214.

Figure 1.

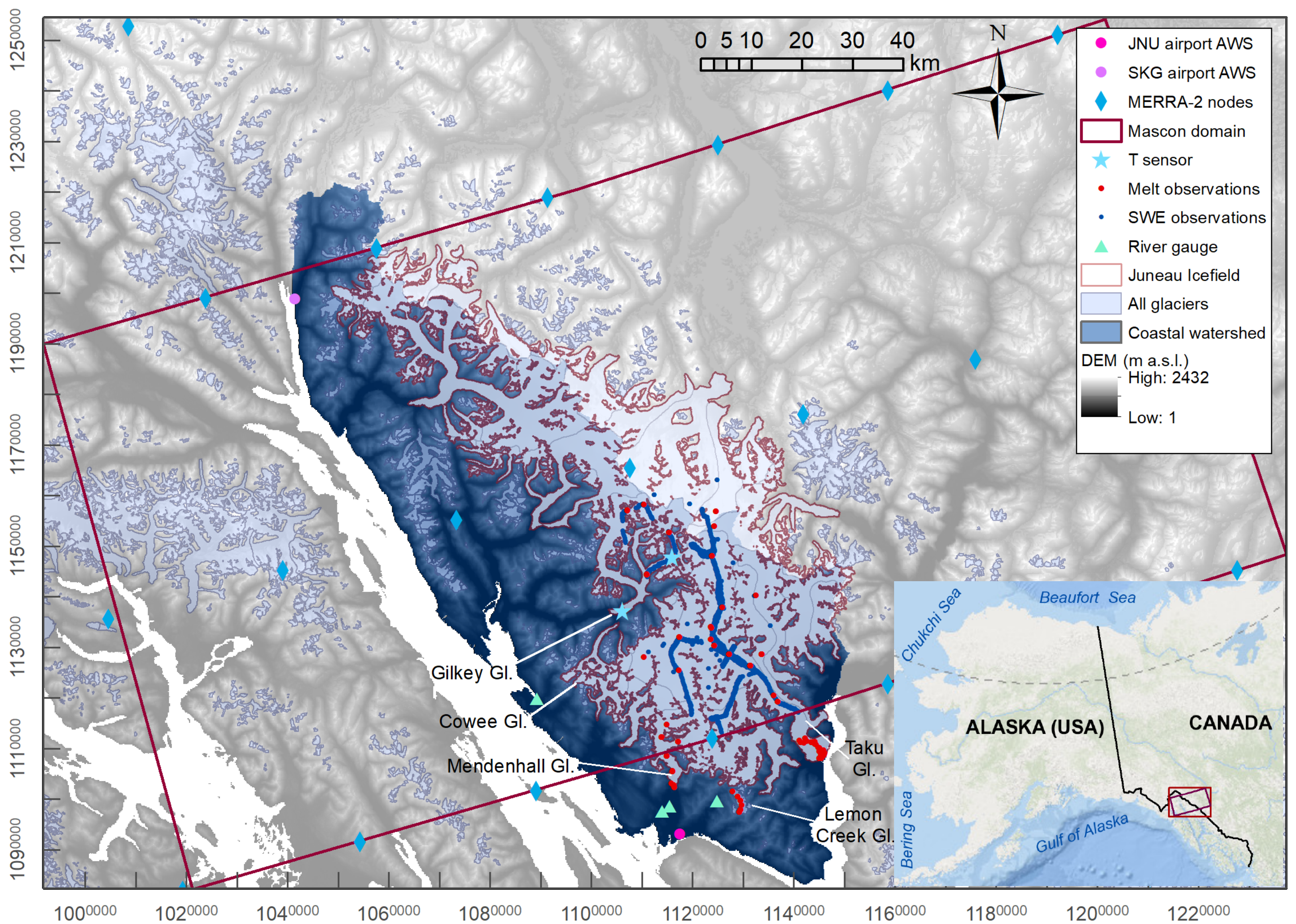

0 5 10 20 30 40 km
N
JNU airport AWS
SKG airport AWS
MERRA-2 nodes
Mascon domain
T sensor
Melt observations
SWE observations
River gauge
Juneau Icefield
All glaciers
Coastal watershed
DEM (m a.s.l.)
High: 2432
Low: 1
Gilkey Gl.
Cowee Gl.
Mendenhall Gl.
Taku Gl.
Lemon Creek Gl.
Beaufort Sea
Chukchi Sea
ALASKA (USA)
CANADA
Bering Sea
Gulf of Alaska
1250000
1230000
1210000
1190000
1170000
1150000
1130000
1110000
1090000
1000000
1020000
1040000
1060000
1080000
1100000
1120000
1140000
1160000
1180000
1200000
1220000

Figure 2.

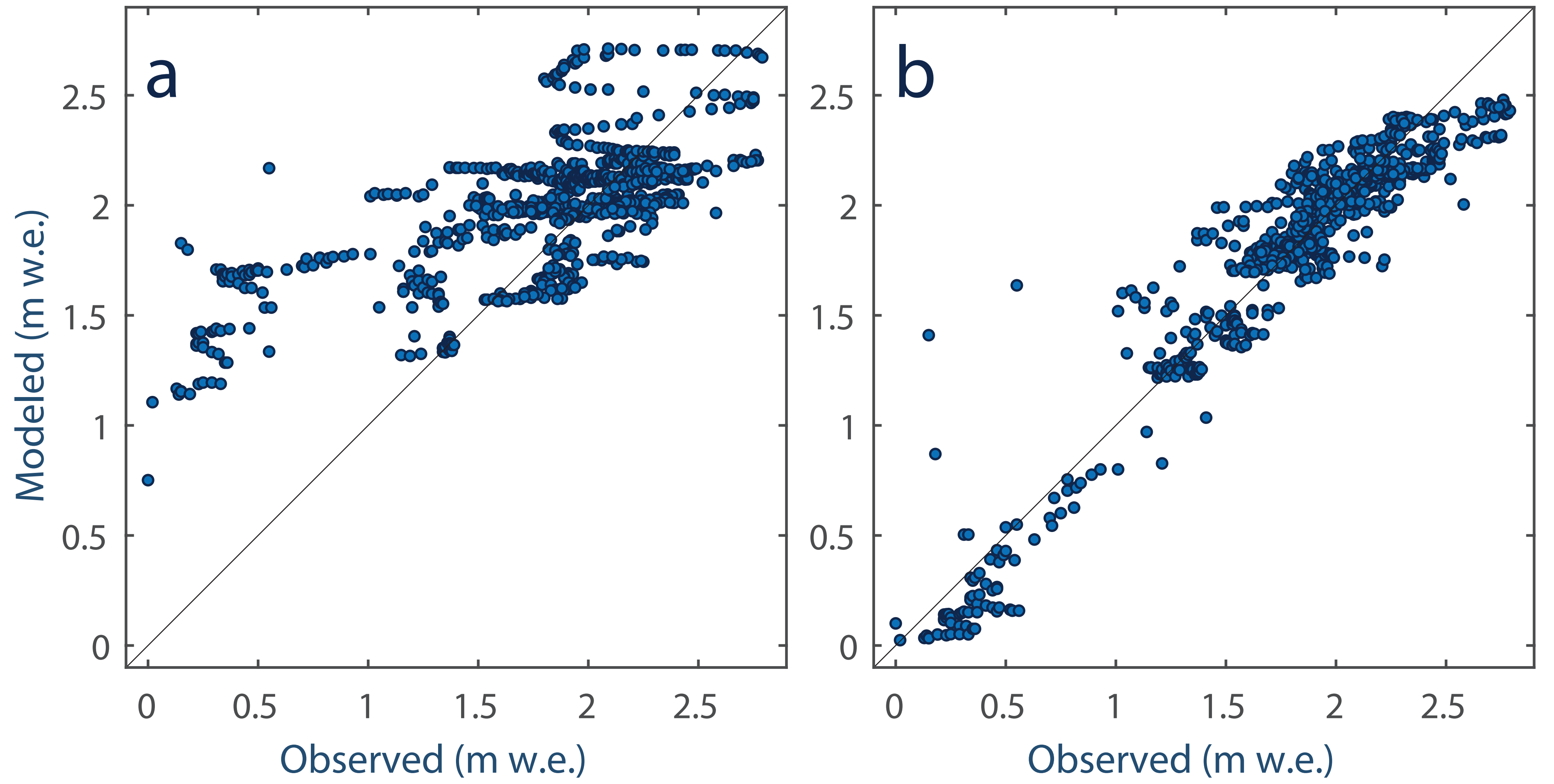
a
b
Modeled (m w.e.)
Observed (m w.e.)
Observed (m w.e.)
0
0.5
1
1.5
2
2.5

Figure 3.

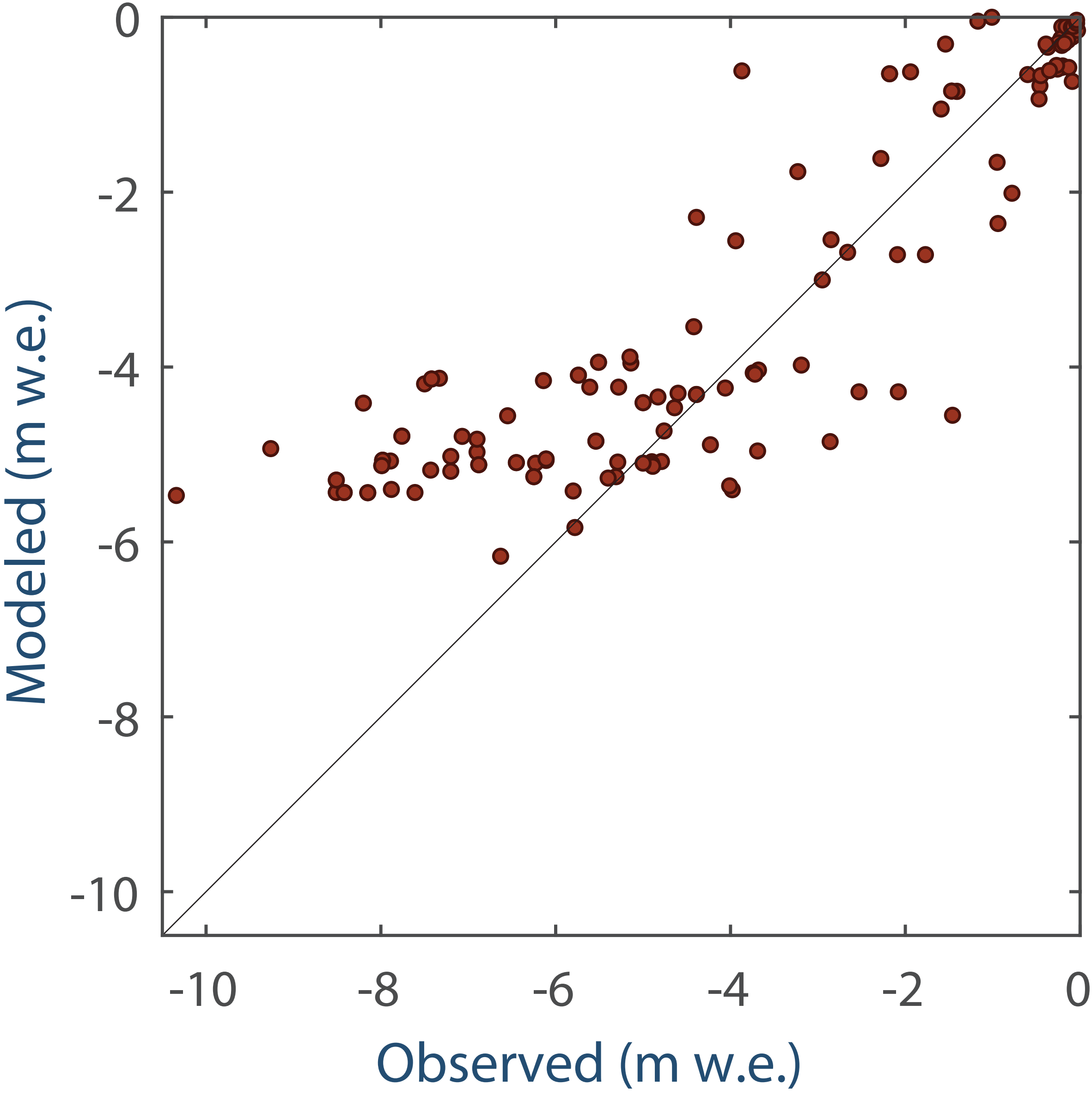

Modeled (m w.e.)
Observed (m w.e.)
0
-2
-4
-6
-8
-10

Figure 4.

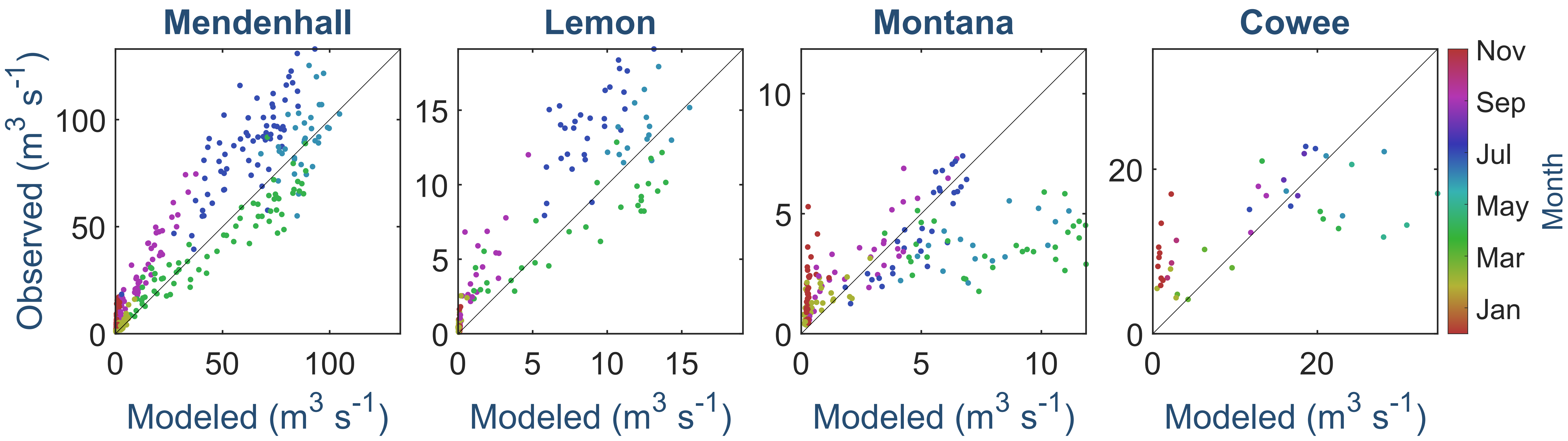
Mendenhall
Lemon
Montana
Cowee
Observed (m3 s-1)
Modeled (m3 s-1)
Nov
Sep
Jul
May
Mar
Jan
Month
0
50
100
5
10
15
20

Figure 5.

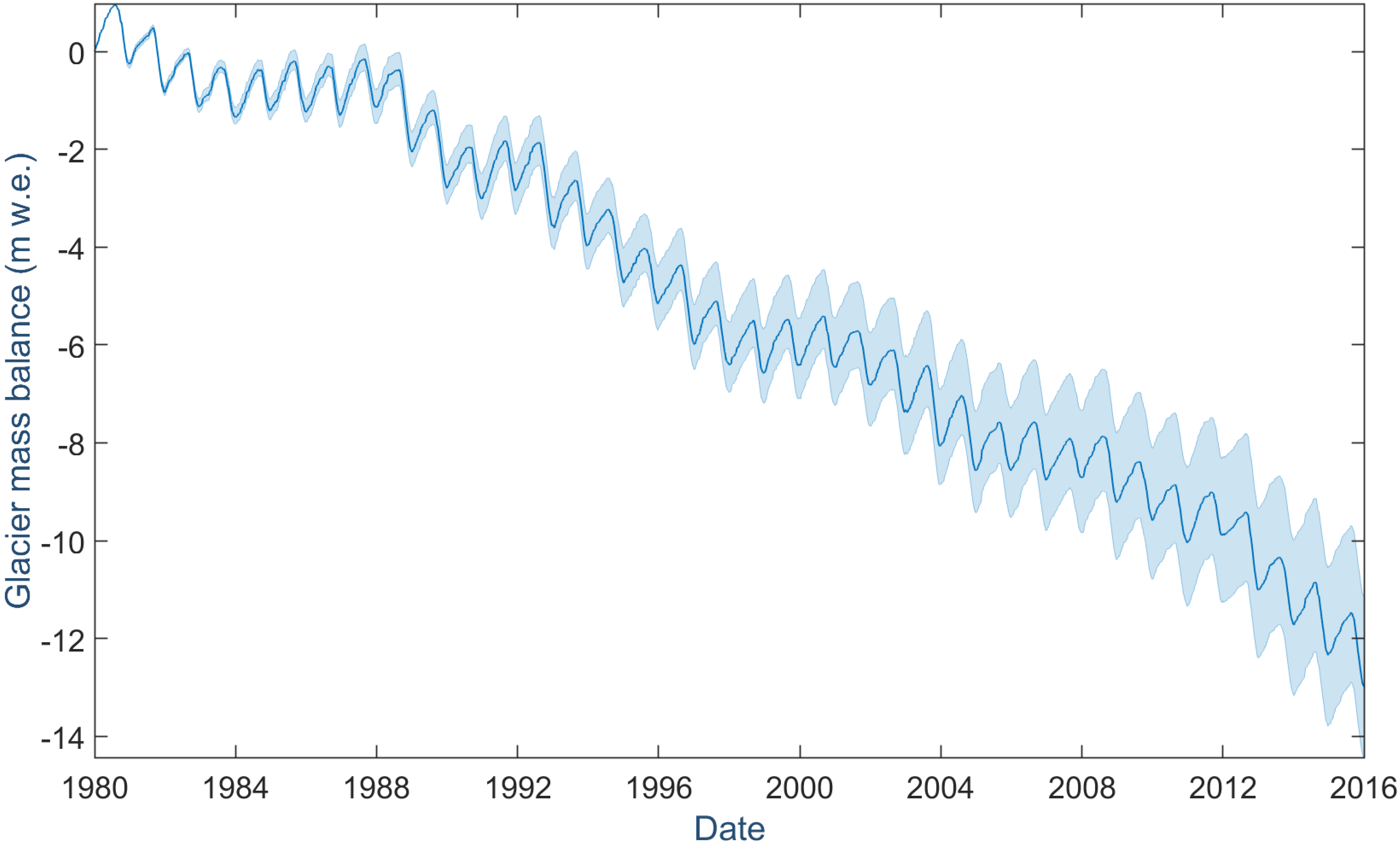
Glacier mass balance (m w.e.)
0
-2
-4
-6
-8
-10
-12
-14
1980
1984
1988
1992
1996
2000
2004
2008
2012
2016
Date

Figure 6.

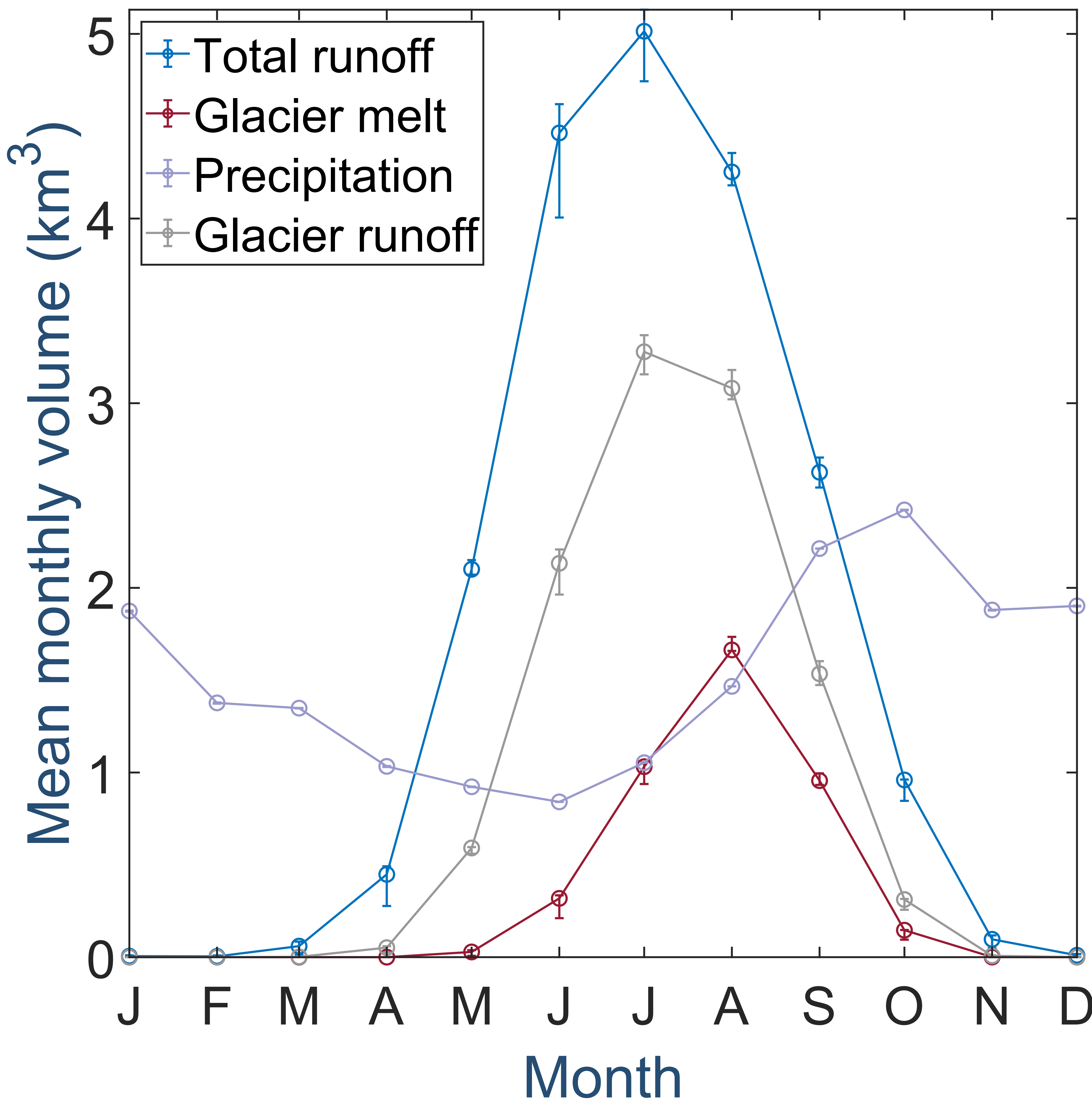

Total runoff
Glacier melt
Precipitation
Glacier runoff
Mean monthly volume (km^3)
0
1
2
3
4
5
J
F
M
A
M
J
J
A
S
O
N
D
Month

Figure 7.

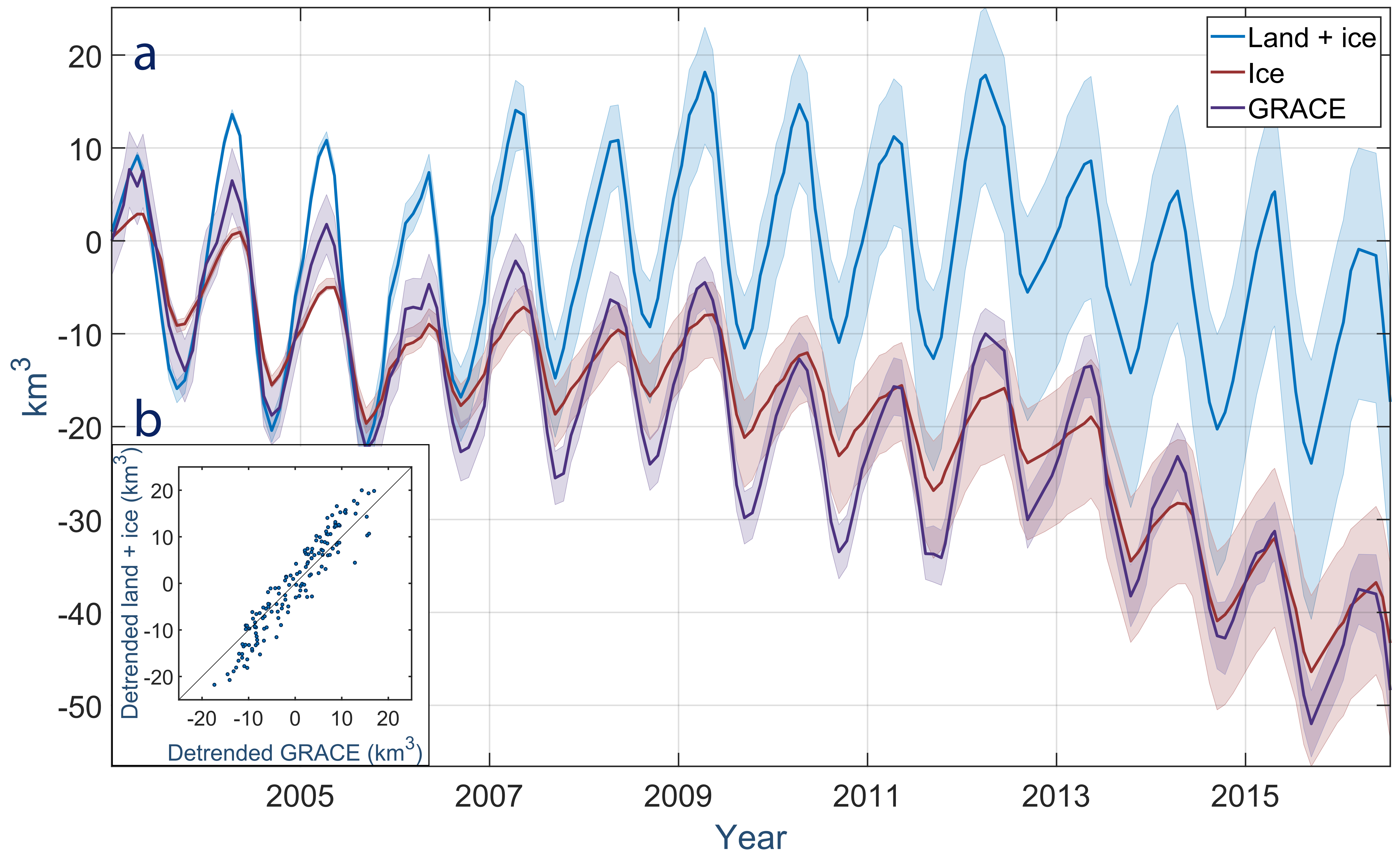

a
b
Land + ice
Ice
GRACE
km^3
Year
20
10
0
-10
-20
-30
-40
-50
2005
2007
2009
2011
2013
2015
Detrended land + ice (km^3)
Detrended GRACE (km^3)
-20
-10
0
10
20

Figure 8.

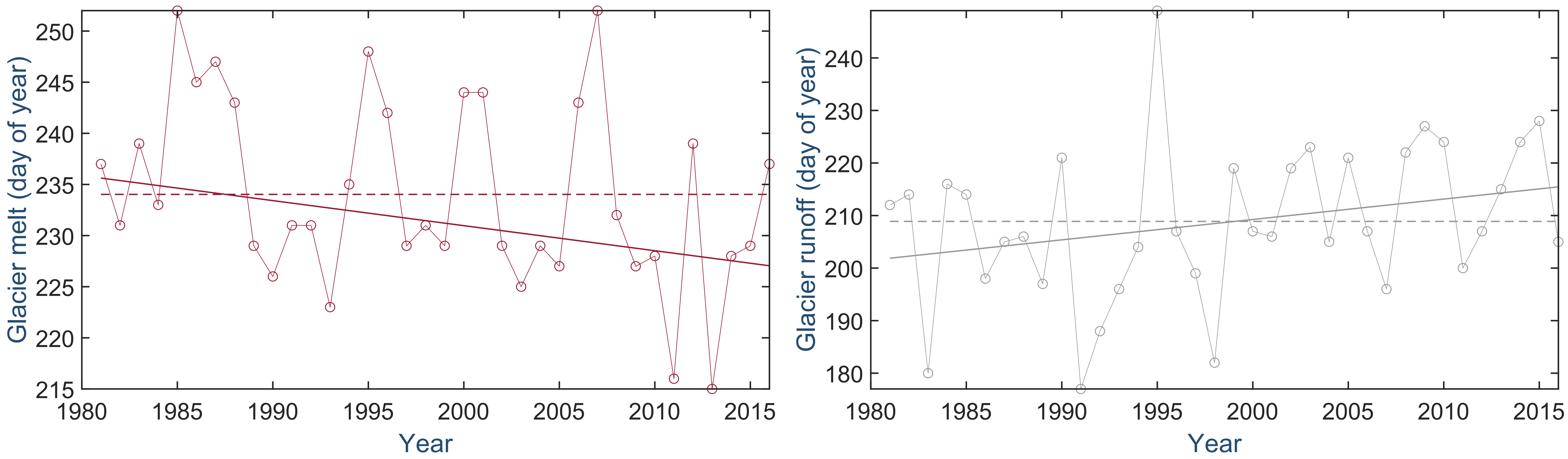

Glacier melt (day of year)
250
245
240
235
230
225
220
215
1980
1985
1990
1995
2000
2005
2010
2015
Year
Glacier runoff (day of year)
240
230
220
210
200
190
180
1980
1985
1990
1995
2000
2005
2010
2015
Year

Figure 9.

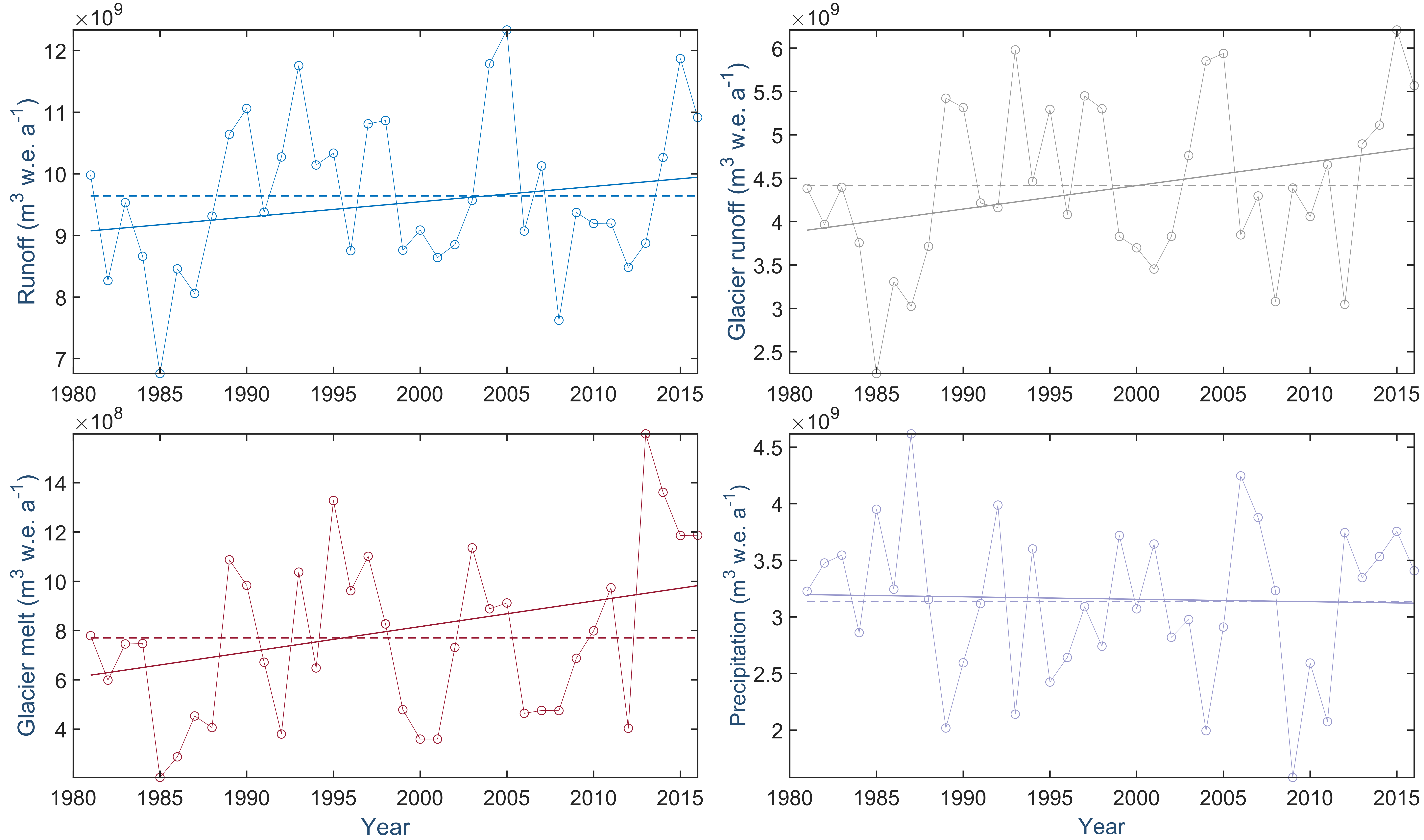

×10^9
Runoff (m^3 w.e. a^-1)
×10^9
Glacier runoff (m^3 w.e. a^-1)
×10^8
Glacier melt (m^3 w.e. a^-1)
×10^9
Precipitation (m^3 w.e. a^-1)
Year
Year

Figure 10.

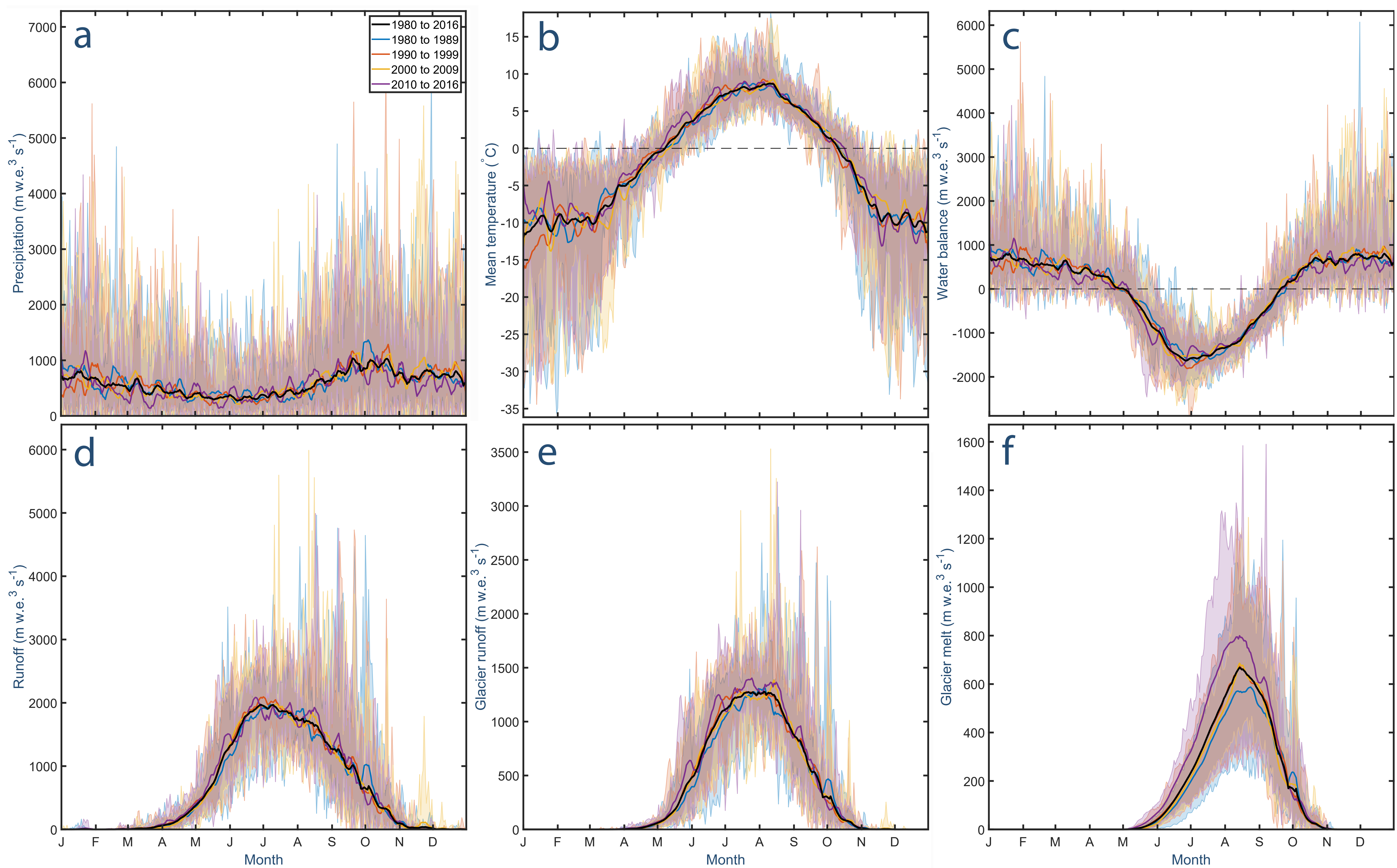

a
b
c
d
e
f
1980 to 2016
1980 to 1989
1990 to 1999
2000 to 2009
2010 to 2016
Precipitation (m w.e.^{3} s^{-1})
Mean temperature (°C)
Water balance (m w.e.^{3} s^{-1})
Runoff (m w.e.^{3} s^{-1})
Glacier runoff (m w.e.^{3} s^{-1})
Glacier melt (m w.e.^{3} s^{-1})
J F M A M J J A S O N D
Month

Figure 11.

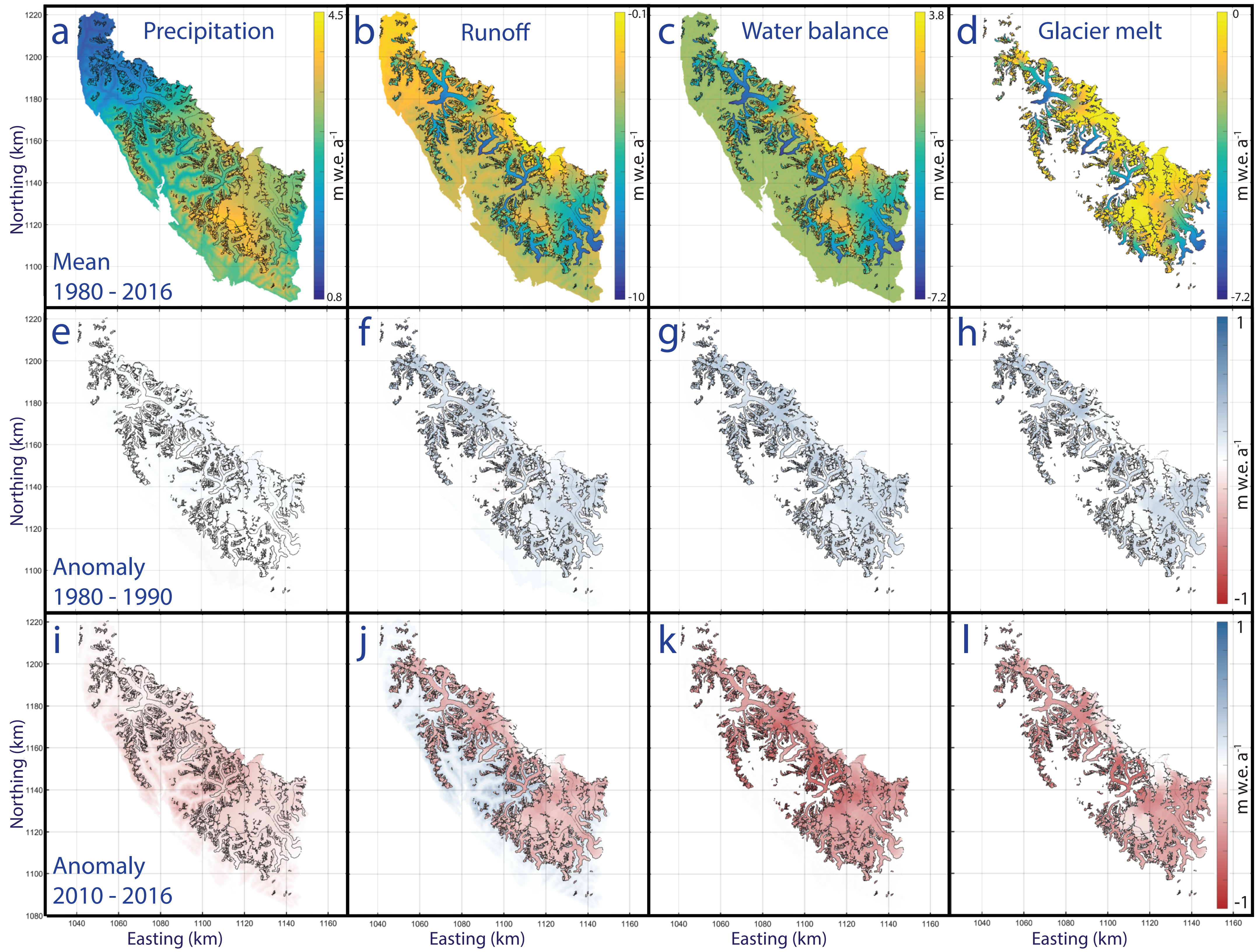

a
Precipitation
b
Runoff
c
Water balance
d
Glacier melt
e
f
g
h
i
j
k
l
Mean
1980 - 2016
Anomaly
1980 - 1990
Anomaly
2010 - 2016
m w.e. a^{-1}
4.5
0.8
-0.1
-10
3.8
-7.2
0
-7.2
1
-1
Northing (km)
Easting (km)
1220
1200
1180
1160
1140
1120
1100
1080
1040
1060
1080
1100
1120
1140
1160